Chapter Three

Phosphate stabilisation experiments

3.1 Introduction

Kinetic column leaching experiments using phosphate coating solutions were considered by this study to be the most suitable experimental method to achieve the primary research objective. Column leaching experiments are a common kinetic test utilised in the mining industry to determine oxidation rates and geochemical reactions that occur in typical mine waste materials (Morin and Hutt, 1997). Column leach experiments can be manipulated to promote specific mechanisms, such as the stabilisation of sulphide mine wastes by phosphate coatings, and was the experimental method chosen by many researchers (Evangelou, 2001; Matlock et al., 2003; Nyavor and Egiebor, 1995; Vandiviere and Evangelou, 1998).

The experimental set-up was devised after an extensive review of the previous research. Phosphate stabilisation was chosen in preference to the use of silicates (Fytas et al., 1999; Zhang and Evangelou, 1998) and organic ligands (Belzile et al., 1997; Chen et al., 1999; Matlock et al., 2003) due to the ease and safety of handling, cost efficiency and commercial availability of phosphate stabilisers. The majority of previously published research into phosphate stabilisation has concentrated on pure iron sulphide samples, pyritic coal wastes or Pb-contaminated soils. The unpublished work of Woltmann (2001) demonstrated the ability of the phosphate stabilisation technique to reduce acid generation and metal release from samples consisting of pure chalcopyrite and arsenopyrite. Three column leaching experiments were contrived to investigate the potential of the phosphate stabilisation technique to prevent acid generation and metal release in: a) polyminerallic, sulphidic mine waste and, b) partly oxidised, polyminerallic mine waste, using liquid and solid phosphate stabilisers on a laboratory scale.

- Experiment 1 – polyminerallic, unoxidised, sulphidic mine waste using liquid phosphate stabiliser.
- Experiment 2 – partly oxidised, polyminerallic mine waste using liquid phosphate stabiliser.
- Experiment 3 – partly oxidised, polyminerallic mine waste using liquid and solid phosphate fertilisers.

Chapter 3 contains the methodology and results for the three phosphate stabilisation experiments. The overall column design and experimental and analytical procedures that were identical for all three experiments are described in a separate experimental methods section after the introduction (Section 3.2). The specific aims, methods and results of each experiment are dealt with in separate sections. The experimental sections are arranged chronologically, allowing observations and conclusions drawn from earlier experiments to be applied to later experiments. A summary of the overall results of the three experiments concludes the chapter.

3.2 Experimental methods

3.2.1 Column Design

All three phosphate stabilisation experiments were conducted as kinetic column leaching experiments using identical column designs (Fig. 3.1). Columns were constructed using polyvinyl chloride pipes of approximately 50 cm length and 5.7 cm internal diameter. Two layers of nylon gauze (grid size 180 µm) and a 2 cm thick layer of glass wool were inserted into the bottom of each column. A layer of pure quartz sand, approximately 2 cm thick, was placed over the glass wool. Plastic funnels were glued to the base of the columns to guide the leachate into 800 ml beakers. Approximately 400 g of the sulphide/sand mixture (experiment 1) or partly oxidised mine waste (experiments 2 and 3) were scooped into the column. Finally, another 2 cm thick layer of pure quartz sand was placed at the top of the column. The layers of quartz sand were placed

above and below the mine waste to prevent the development of preferential flow channels in the columns. The quartz sand was washed with 1 M HCl to ensure purity and then flushed repeatedly with distilled water to rinse out the HCl before being placed into the columns.

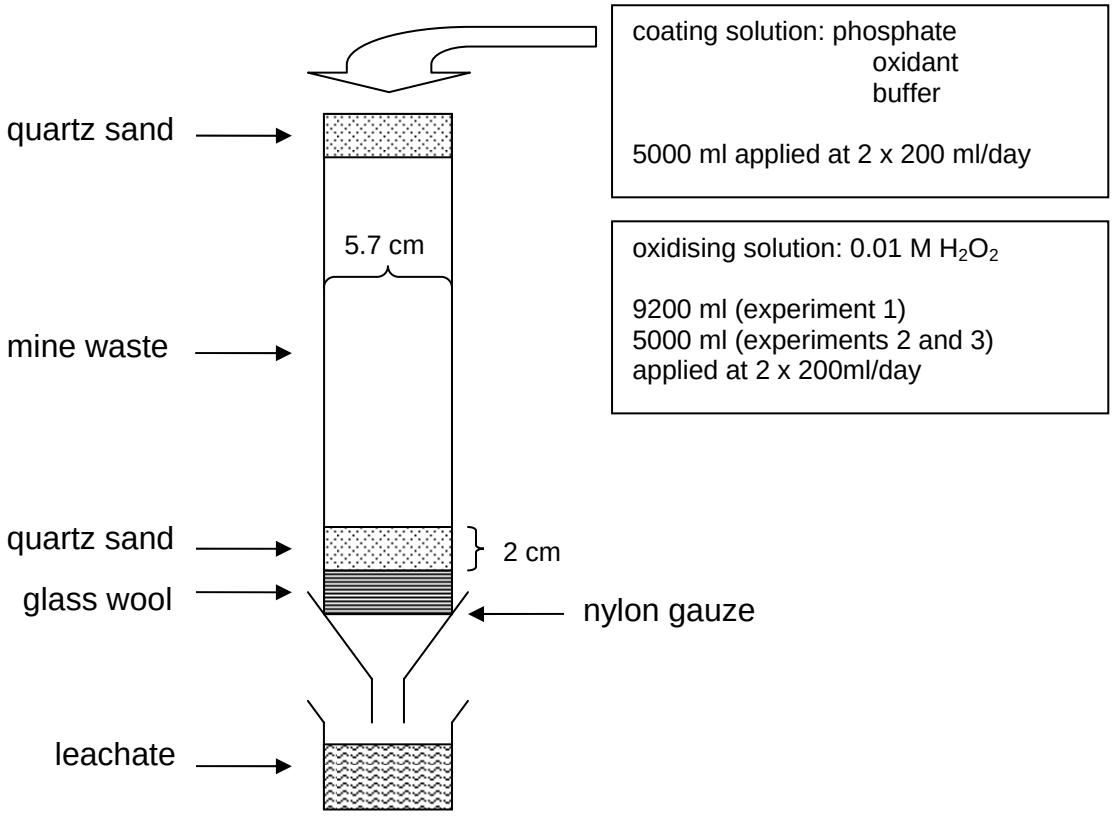

Figure 3.1. Diagram of the column design used in the phosphate stabilisation experiments.

Mine waste material used in the columns was sourced from the abandoned Montalbion silver mine, far north Queensland (Chapter 2). Random sulphide-rich grab samples and composite mine waste samples were collected from waste dump faces (Fig. 2.1). The waste material was crushed in a steel jaw crusher and sieved, with the >2 mm and <10 mm fraction being retained. The waste material was then mixed thoroughly until homogeneity was achieved and quartered to ensure the material in each column was, for all practical purposes, identical. Representative samples of the waste material were pulverised in a chrome-steel mill and split, with one fraction being analysed by X-ray fluorescence spectrometry (XRF), the other by XRD at the JCU AAC (results in

Appendix B1). Details of the preparation of the waste material specific to each experiment are described in the separate experimental methods sections.

3.2.2 Experiment design

The experiments were conducted in two stages, a coating stage and a dissolution stage. In the coating stage of each experiment the columns were leached with 5000 ml of coating solution at a rate of 400 ml per day (2 x 200 ml aliquots) for 13 days. The application rate of the coating solution was adequate to saturate the material in the columns throughout the experiment. The coating solution consisted of a phosphate source, an oxidant and 0.2 M sodium acetate (CH_3COONa) (NaAC) to act as a buffer. The solutions were buffered as it has been established that the solution pH must be above 5 to form Fe phosphates on pyrite (Evangelou, 1995a). Details of the coating solutions specific to each experiment are described in the separate experimental sections. After the addition of 5000 ml of coating solution, the columns were leached with two 250 ml aliquots of $Ca(OH)_2$ over a period of 24 hours. The $Ca(OH)_2$ was added to stabilise any phosphate coatings in the columns and to raise the pH. Two hours after the final $Ca(OH)_2$ addition, small aliquots (~30 g) of the waste material were carefully removed from each column and prepared for SEM and EDS investigations at the JCU AAC.

In the dissolution stage of all three experiments, the coated columns were leached with an oxidising solution of 0.01 M H_2O_2 at the rate of 400 ml per day (2 X 200 ml aliquots) until the addition of 9200 ml (experiment 1) or 5000 ml (experiments 2 and 3) of oxidising solution. Control columns were added to the dissolution stage of experiments 1 and 2, containing uncoated sulphidic mine waste and partly oxidised mine waste, respectively. The control column of experiment 2 was also used as the control for experiment 3 as the waste material used in both experiments and the conditions under which they were performed (temperature and humidity) were identical. The dissolution stage was designed to test the stability of any developed phosphate phases in an oxidising environment and their effectiveness in preventing further sulphide oxidation. H_2O_2 was used as the oxidant in experiments 1 and 2 because of the extreme

oxidising environment it creates, thus allowing relatively short-term dissolution experiments to simulate much longer oxidation periods under natural conditions (Georgopoulou et al., 1996). At the completion of the dissolution stage, the columns were dismantled and a sample (~50 g) from each column was prepared for investigation with SEM and EDS at the JCU AAC.

3.2.3 Analytical methods

Throughout both stages of all three experiments, the leachate temperature, pH and conductivity of each 200 ml aliquot was measured. The pH was measured in the receiving beaker using a Radiometer Copenhagen PHM210 pH meter with an Ag/AgCl electrode whilst the sample was being stirred by a Variomag magnetic stirrer and bead. The conductivity was measured using a Hanna H98303 handheld conductivity meter with a 2000 µS/cm upper detection limit. Dilution of the coating stage leachates by a factor of up to 50 times was required due to high conductivities of the coating solution.

Leachate samples were stored under refridgeration at 4^{o} C. Precipitates were observed in several of the leachates, therefore selected samples were decanted, but not filtered, before being analysed by ICP-MS and ICP-AES at the JCU AAC, Townsville. Specific sampling regimes and elements analysed are detailed in the separate experimental sections (Sections 3.3.2, 3.4.2 and 3.5.2). Detection limits of elements varied between experiments due to varying dilution factors necessitated by the nature of the coating solutions.

The samples of waste material collected from the columns at the completion of the two experimental stages were inspected underneath a binocular microscope. Ten to 20 representative grains from each sample were chosen for SEM and EDS investigation. The grains were mounted on SEM stubs and carbon-coated to promote conductivity. Polished blocks were not investigated as Woltmann (2001) ascertained that the phosphate phases formed were too thin and/or fragile to survive the polished block making process. The lack of grains with flat surfaces prevented quantitative EDS analysis, allowing only general bulk chemistries of the analysed surficial phases to be determined.

SEM observations were performed on a Jeol JSM-6300 scanning electron microscope and EDS measurements were taken with a Moran Scientific V8.5 Multi Channel Analyser at the AAC, JCU, Cairns. Selected samples were gold-coated for SEM photography, which was undertaken on a Jeol JSM-5410LV scanning electron microscope at the AAC, JCU, Townsville.

3.3 Phosphate stabilisation of polymineralic, sulphidic mine waste using liquid chemical stabilisers (experiment 1)

3.3.1 Aims

The aims of experiment 1 were:

a) to determine the morphologies and chemistries of any phosphate phases formed by the interaction of polymineralic, sulphidic (i.e. unoxidised) mine waste with liquid phosphate stabilisers;

b) to determine the stability, metal attenuation ability and acid generation inhibition ability of any phosphate phases formed by the interaction of polymineralic, sulphidic (i.e. unoxidised) mine waste with liquid phosphate stabilisers.

3.3.2 Specific methodology

Sulphide-rich Montalbion mine waste material was handpicked to generate a polymineralic, sulphidic mine waste with representative ratios of the major sulphide minerals present in the Montalbion waste dump (galena > sphalerite > chalcopyrite > tetrahedrite > pyrite > arsenopyrite). The XRD trace of the sulphidic mine waste revealed the presence of an appreciable amount of anglesite (Appendix B1). In order to ensure the majority of the waste material was comprised of sulphides and quartz, the columns were washed with 10 x 200 ml flushes of 1 M HCl, which removed the majority of any soluble secondary oxidation products present in the waste material. Anglesite was reduced to levels below detection by XRD (Appendix B1). However, SEM observation of HCl-washed grains revealed a small number of euhedral

anglesite crystals and traces of unidentified Cu and Fe sulphates. Residual sulphates persisted due to kinetic factors, the short HCl residence time failing to completely dissolve larger crystals. Following HCl washing, the columns were then flushed with distilled water until all HCl was removed from the columns. The HCl-washed sulphidic mine waste was mixed with pure HCl-washed quartz sand at a 1:1 ratio to increase the porosity of the material.

The compositions and concentrations of the coating solutions used in experiment 1 were prepared using the protocols of Fytas and Evangelou (1998) (Table 3.1).

Table 3.1. Coating solutions used in the coating stage of experiment 1.

	Oxidant	Phosphate	Buffer
Column A	0.01 M H_2O_2	0.2 M KH_2PO_4	0.2 M CH_3COONa
Column B	0.01 M H_2O_2	0.4 M KH_2PO_4	0.2 M CH_3COONa
Column C	0.1 M H_2O_2	0.4 M KH_2PO_4	0.2 M CH_3COONa
Column D	0.2 M H_2O_2	0.2 M KH_2PO_4	0.2 M CH_3COONa

Five litres of coating solution were added to the respective columns at a rate of 400 ml per day. During the coating stage, leachate samples were collected after the addition of 1200 ml, 3000 ml and 5000 ml of coating solution. These leachates were analysed for Ag (5 µg/l), Al (100 µg/l), As (1 µg/l), Ca (100 µg/l), Cd (5 µg/l), Cu (0.1 µg/l), In (5 µg/l), Mg (10 µg/l), Mn (10 µg/l), Pb (0.05 µg/l), Sb (0.1 µg/l), Se (100 µg/l), and Zn (5 µg/l) by ICP-MS and for Fe (100 µg/l), K (1 mg/l), Na (0.5 mg/l), S (1 mg/l) and Si (1 mg/l) by ICP–AES. Detection levels are shown in brackets.

The results of Woltmann (2001) indicated a steady decrease in the coated column leachate pH throughout the dissolution stage. In order to discover whether leachate pH would stabilise or continue to decrease, the dissolution stage of experiment 1 was run until the coated column leachate pH's either stabilised or decreased to the control column leachate pH. The dissolution

stage was halted after the addition of 9200 ml of 0.01 M H_2O_2 at a rate of 400 ml per day. Leachate samples were collected after the addition of 400 ml and then every 1200 ml addition until the addition of 9200 ml of oxidant. These samples were analysed for As, Cu, Pb, Sb and Zn by ICP–MS and Fe and S by ICP–AES (detection levels as above).

3.3.3 Coating stage results

The XRD and bulk XRF results for the sulphidic waste material used in the columns of experiment 1 are tabulated in Appendix B1. Small quantities of off-white precipitate were observed in initial coating stage leachates of all columns. The precipitates were mostly fine-grained quartz sand particles, though some iron precipitates were probably responsible for the discolouration. The leachates became clear after ~1000 ml of coating solution addition. Complete chemical results for the coating stage leachates are tabulated in Appendix B2.

Leachate chemistry

The column leachates were buffered to pH values of 5 to 5.7 throughout the coating stage of the experiment (Fig. 3.2a). The coating solutions were therefore above the minimum pH required for stable phosphate phases to form (Evangelou, 1994). Several jumps in the leachate pH occurred during the coating stage. Reference measurements of buffer solutions showed similar jumps, proving that the jumps in the leachate pH readings were caused by instrumental error. Despite these problems, pH drift for individual columns for the duration of the coating stage was restricted to 0.4 of a pH unit. Instrumental problems caused 0.2 pH units of that drift, therefore pH drift for each column leachate was limited to 0.2 pH units during the coating stage (Fig. 3.2a). The pH values of column B and C leachates were lower than column A and D leachates as they contained twice the concentration of KH_2PO_4 (Table 3.1). This is a result of acid production from KH_2PO_4 disassociation:

$$KH_2PO_{4(aq)} \rightarrow K^+_{(aq)} + 2H^+_{(aq)} + PO_4^{3-}{}_{(aq)} \qquad (3.1)$$

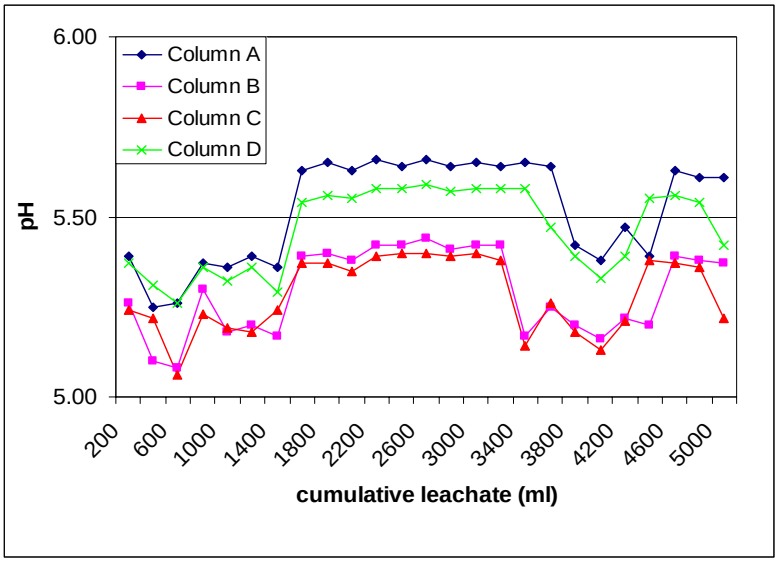

Figure 3.2a.

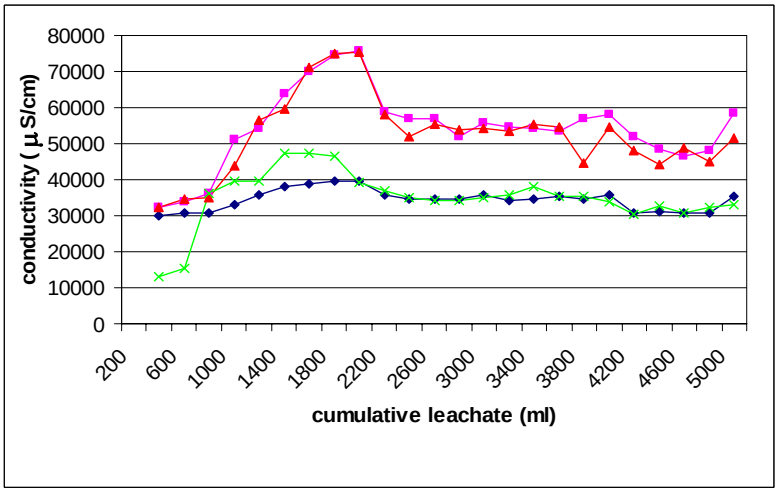

Figure 3.2b.

Figure 3.2. Experiment 1 pH (a) and conductivity (b) of coating stage leachates. Legend for (a) also applies to (b).

The coating solutions had high conductivities (~34000 µS/cm, columns A and D; ~48000 µS/cm, columns B and C) before they were passed through the columns due to disassociation of KH_2PO_4 and NaAC (Table 3.1). Leachate conductivities rose to values as high as 75 000 µS/cm before stabilising at values close to the conductivities of the original coating solutions (Fig. 3.2b). The conductivities of column B and C leachates were generally around 1.5 times the conductivities for leachates from columns A and D due to the stronger KH_2PO_4 concentrations in columns B and C (Table 3.1).

The Ag, Fe, In, Mg, Mn and Se concentrations in the coating stage leachates were below detection in all columns. Aluminium and Ca were below, or close to detection levels in all column leachates. Sodium and K concentrations were high in all columns throughout the coating stage due to the presence of NaAC and KH_2PO_4 in the coating solutions. The concentrations of all other elements generally decreased through the course of the coating stage (Fig. 3.3). The reduction in element concentration during the coating stage varied between 80 % (As) to 13 % (Cd). Such decreases also varied greatly between columns, particularly for Cu (14 % decrease in column B; 58 % decrease in column D) and Zn (16 % decrease in column B; 58 % decrease in column D). The overall order of decrease in elemental concentration during the coating stage (average of the four columns) was As > SO_4^{2-} > Si > Pb > Cu > Zn > Sb > Cd. Disregarding the elements added as part of the coating solution, the overall elemental abundance in the coating stage column leachates (average of the four columns' cumulative element release throughout the coating stage) was SO_4^{2-} > Cu > Zn > As > Si > Sb > Pb > Cd > Al > Ca > Ag, Fe, In, Mg, Mn and Se. The order of elemental abundance in the bulk XRF results of the polyminerallic, sulphidic waste (after the HCl washing) was Si > S > Pb > Cu > Fe > Zn > Sb > Al > As > Mg > In > Cd > Se > Ca > Mn (Appendix B1). Comparing this with the elemental abundance in the coating stage leachates, it is apparent that Si, Pb and Fe were relatively immobile during the coating stage, whereas As, Zn and Cd were relatively mobile during the coating stage.

SEM observations

Complete saturation of the material in the columns was noted when the representative aliquots were removed for SEM observation. No visible evidence of preferential flow path development was noted. There was no visible difference in phosphate formation between the top and the bottom of the columns. A summary of the post-coating stage SEM observations is presented in Table 3.2. Detailed results and additional SEM micrographs are presented in Appendix B5. The order of extent of phosphate formation in the coated columns

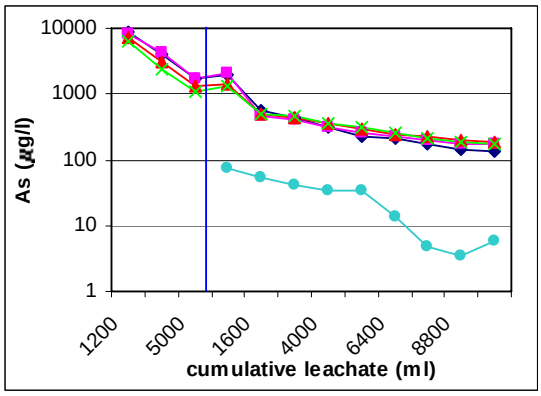

Figure 3.3a. As

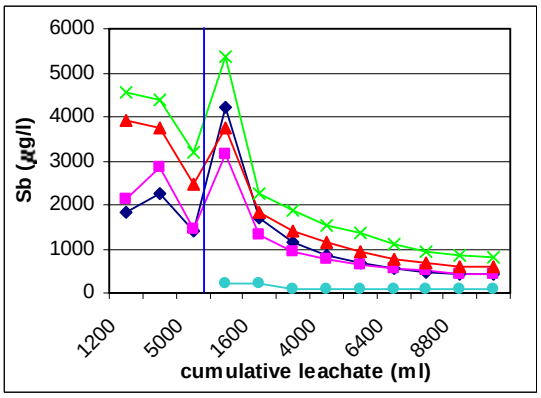

Figure 3.3b. Sb

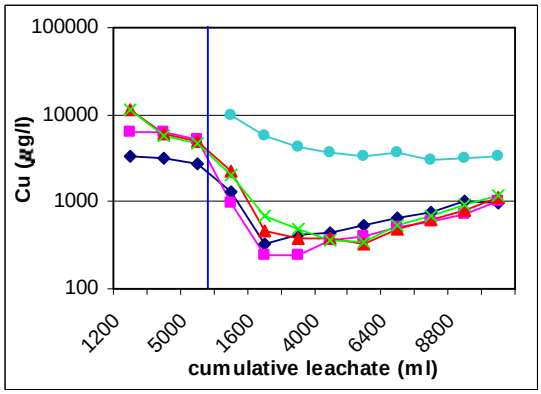

Figure 3.3c. Cu

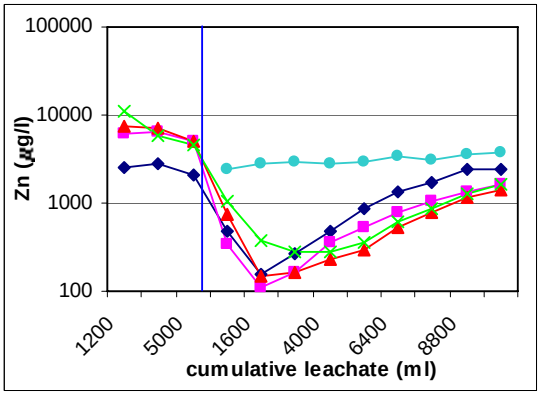

Figure 3.3d. Zn

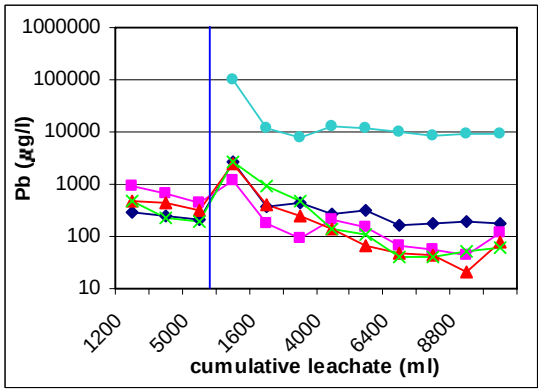

Figure 3.3e. Pb

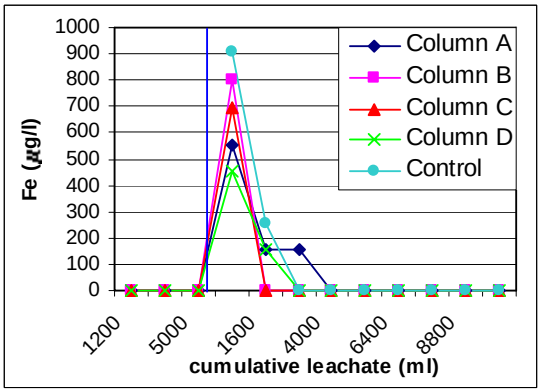

Figure 3.3f. Fe

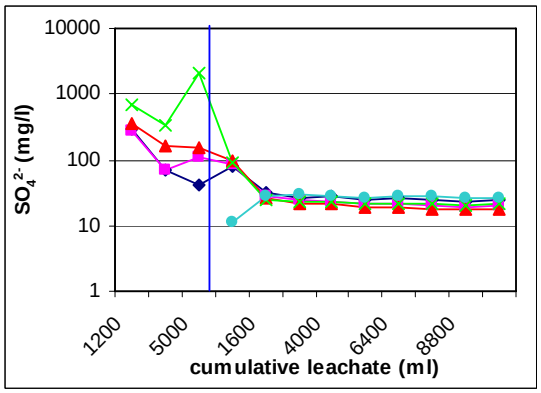

Figure 3.3g. SO_4^{2-}

Figure 3.3. Concentrations of elements in leachates of experiment 1. Legend for (f) applicable to all graphs. Vertical line represents addition of $Ca(OH)_2$ and separates coating stage results (left of the line) from dissolution stage results (right of the line).

was: column D > column C >> column B > column A (based on visual estimation). This applied to all phosphate species observed. Two major forms of phosphate phase were observed. Firstly, an “amorphous” (see definitions), occasionally layered Fe–K±Cu phosphate, which formed a coating on chalcopyrite (Fig. 3.4a,b,d) and, to a lesser extent, pyrite and arsenopyrite. Secondly, metal ± alkali phosphate crystals which formed isolated precipitates or coalescences, usually on, but not restricted to, their parent sulphide (e.g. Pb phosphate on galena (Fig. 3.4c); Zn phosphate on sphalerite (Fig. 3.4b)). Galena hosted the most extensive precipitates in all columns, whereas chalcopyrite was extensively coated by the amorphous Fe–K phosphates. In contrast to previous research (cf. Evangelou, 1994, 1995b; Huang and Evangelou, 1994), pyrite was rarely and poorly coated (Fig. 3.4a). Tetrahedrite was uncoated and only rarely hosted phosphate precipitates. The phosphate coatings, regardless of thickness, displayed a network of cracks which are interpreted to be a result of desiccation during sample preparation or under the vacuum of the SEM (Jones et al., 2003). Late Ca, Cu, Pb, Pb-As and Zn sulphate precipitates were observed in columns C and D.

3.3.4 Dissolution stage results

Leachate chemistry

Complete chemical results for the dissolution stage leachates are tabulated in Appendix B2. The control column leachate pH initially dropped to 3.5, then steadily rose, stabilising at a value of 4.15. This demonstrates the acidic nature of the sulphidic waste material (Fig. 3.5a). The addition of $Ca(OH)_2$ stabiliser between the end of the coating stage and the start of the dissolution stage raised the pH of the coated column leachates to around 7.5. The pH of the coated column leachates dropped steadily until the rates of pH decline diverged after 3000 ml of oxidising solution addition. The pH then declines more rapidly in Column A and B leachates than in column C and D leachates. The column leachates had stabilised by the conclusion of the experiment to approximate pH values of: control column, 4.1; column A, 4.9; column B, 5.5; column C, 5.9; column D, 5.9 (Fig. 3.5a).

Table 3.2. Summary of SEM observations of precipitates and coatings formed on polyminerallic, sulphidic mine waste in columns during the coating stage of experiment 1.

Chemistry	Morphology	Abundance
Pb±Ca phosphate (Fig. 3.4c)	pincushions of fine (0.5 µm x 10 µm) acicular crystals often form extensive coalescences; large (100 µm x 10 µm) acicular crystals contain Ca	pincushions cover >75 % of galena in columns A and B, 100 % of galena in columns C and D; large crystals are rare precipitates in columns C and D
Cu-Ca±K phosphate (Fig. 3.4a,b,d)	scattered spherical rosettes of ~10 µm diameter, often form coalescences of radial acicular splays in columns C and D	cover <5 % of chalcopyrite surfaces in columns A and B; cover <20 % of Fe phosphate-coated chalcopyrite surfaces in columns C and D
Fe-K±Cu phosphate (Fig. 3.4a,b,d)	amorphous coating with extensive desiccation cracks, often layered in columns C and D	thin coating on <1 % of chalcopyrite in columns A and B; thick coating on ~95 % of chalcopyrite and thin coating on <5 % of pyrite and arsenopyrite in columns C and D
Zn-K±Ca phosphate (Fig. 3.4b)	large (100 µm x 10 µm) bladed crystal precipitates; radial flow-like agglomerations of very fine-grained (100 nm x 10 nm) acicular crystals	bladed crystals rare precipitates in columns A and B, more common in columns C and D; flow-like agglomerations cover ~50 % of sphalerite in columns C and D only
Ca±K, Si, S, Fe phosphate	agglomerations of very fine grained (1 µm x 0.1 µm) needles and rare botryoids	rare precipitates on <1 % of grains in columns A and B; <5 % of grains in columns C and D; no preferential substrate
Pb, Pb-As, Cu, Fe and Ca sulphates	euhedral rosettes or splays of crystal precipitates	rare isolated precipitates in columns C and D

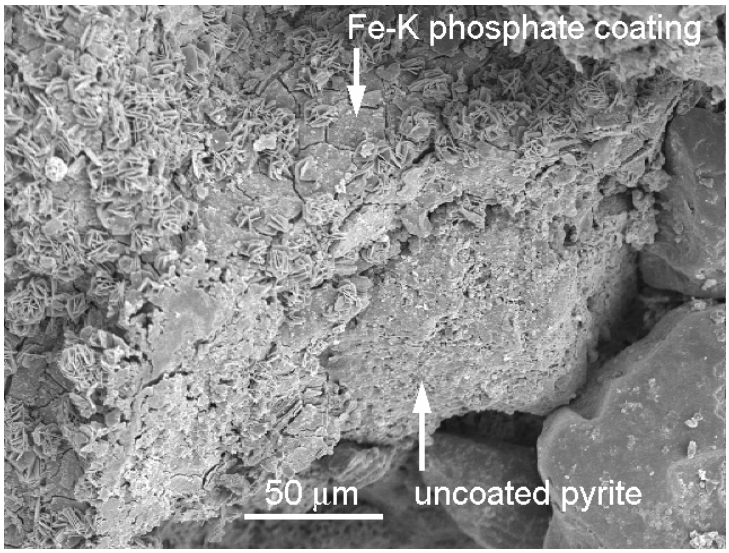

Figure 3.4a.

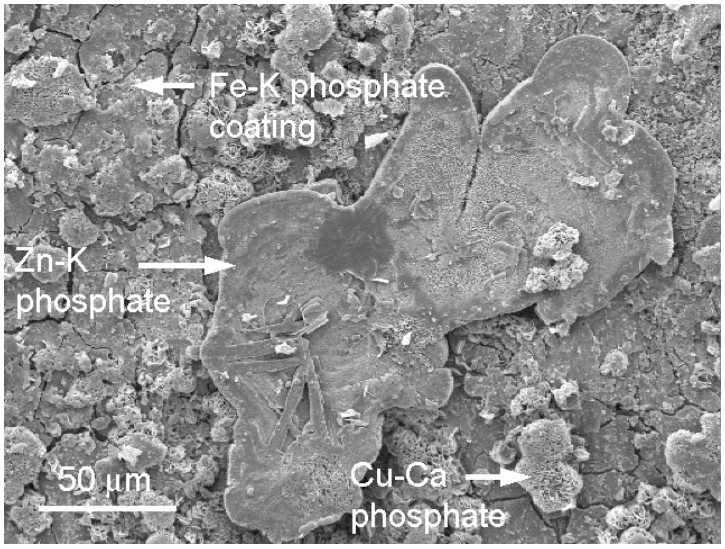

Figure 3.4b.

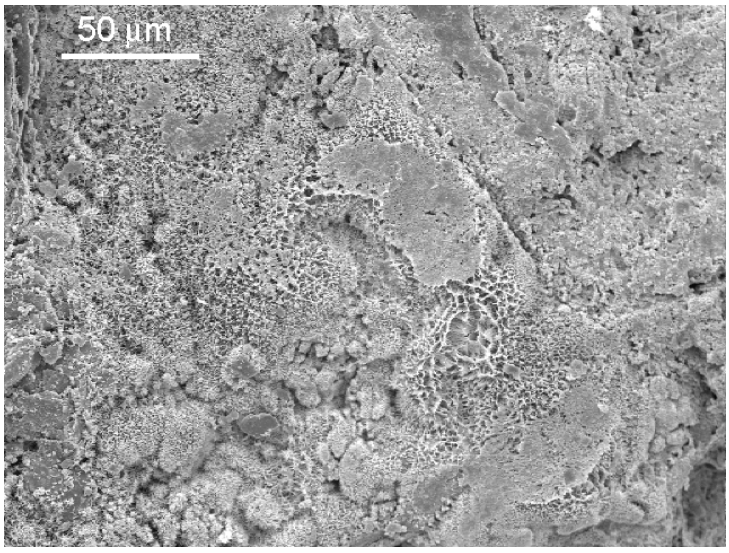

Figure 3.4c.

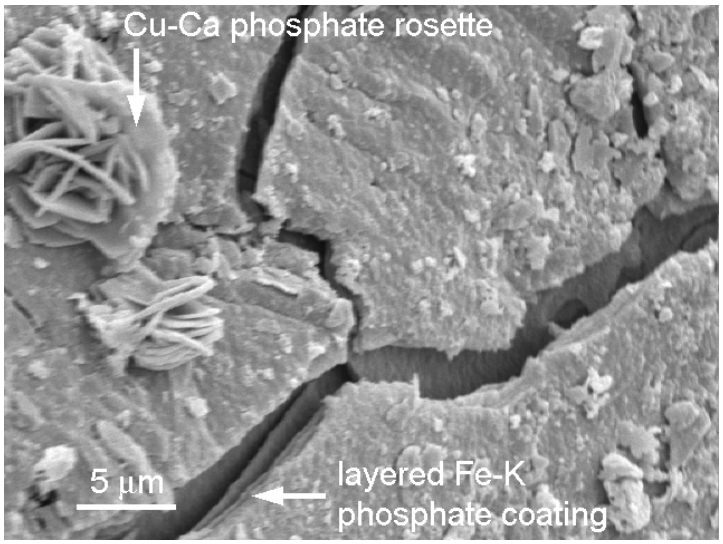

Figure 3.4d.

Figure 3.4. SEM micrographs of material removed from the coated columns after the coating stage of experiment 1. a) Fe-K phosphate on chalcopyrite with adjacent uncoated pyrite, column D. b) Flow like agglomeration of Zn-K phosphate precipitated on scattered Cu-K phosphate rosettes and Fe-K phosphate coating, column C. EDS trace of Zn-K phosphate in Appendix B8. c) Coalescence of Pb phosphate pincushions, column A. d) Layered Fe-K phosphate coating and isolated Cu-K phosphate rosettes, column D.

The coated column leachates initially had high conductivities (400–700 μS/cm) (Fig. 3.5b). These values dropped rapidly, stabilising at values of 60-70 μS/cm after the addition of 5000 ml of oxidising solution. The control column had an initial conductivity of 160 μS/cm, which rose abruptly to 539 μS/cm before dropping rapidly and stabilising at ~80 μS/cm, slightly higher than the coated columns.

Two distinct trends were identified in the column leachate chemistry results. Firstly, the base metal concentrations in the coated column leachates were lower than the control column leachates, by two orders of magnitude in the case of Pb (Fig. 3.3c,d,e). Secondly, the concentrations of As and Sb in the coated column leachates were higher than the control column leachate As and Sb concentrations (Fig. 3.3a,b). Generally, element concentrations were initially relatively high in all column leachates and rapidly dropped before stabilising at much lower values. There were four exceptions to this; 1) the As and Sb concentrations of the control column leachates, which dropped steadily

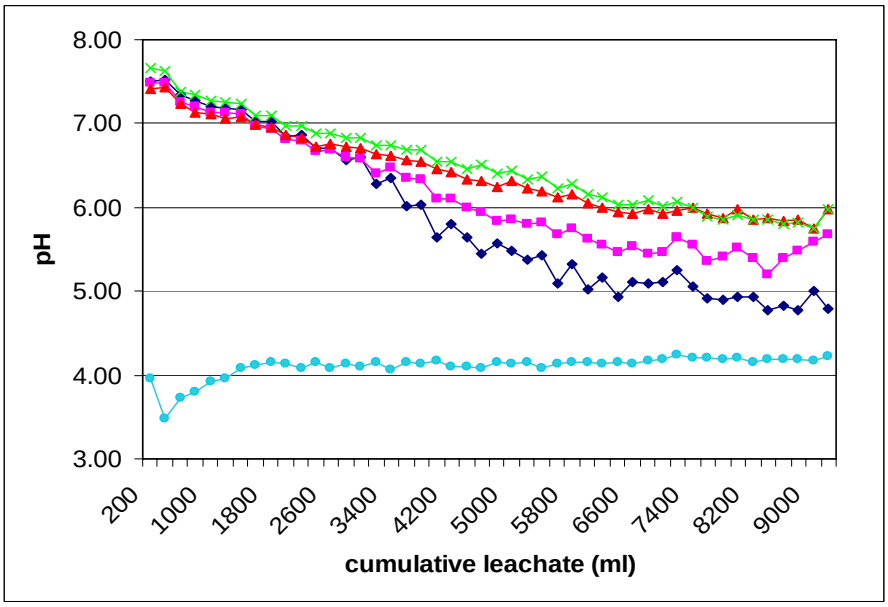

Figure 3.5a.

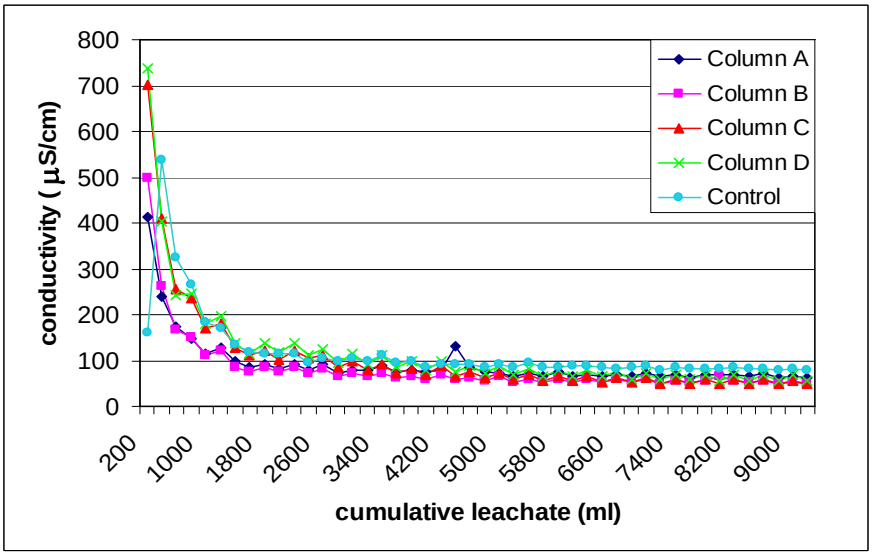

Figure 3.5b.

Figure 3.5. Experiment 1 pH (a) and conductivity (b) of dissolution stage leachates. Legend for (b) also applies to (a).

throughout the dissolution stage (Fig. 3.3a,b); 2) the SO_4^{2-} concentration of the control column leachates, which initially rose before stabilising (Fig. 3.3g); 3) the Zn concentration of the control column leachates, which rose steadily throughout the dissolution stage (Fig. 3.3d) and; 4) the Cu and Zn concentrations of the coated column leachates, which initially dropped, then

rose with additional oxidising solution addition, Cu steadily and Zn rapidly (Fig. 3.3c,d). Dissolved element concentration trends between the four coated column leachates showed very little variation, except for column A [Zn], which rose significantly higher than the other coated columns (Fig. 3.3d). The relative elemental abundance in the dissolution stage column leachates (average of the four columns' cumulative element release throughout the coating stage) was SO_4^{2-} > Sb > Zn > Cu > As > Pb > Fe. This differs significantly from the relative cumulative elemental abundance in the control column leachates, which was Pb > SO_4^{2-} > Cu > Zn > Fe > Sb > As.

The control column leachate [SO_4^{2-}] appeared anomalously low in comparison to the coated column leachate values (Fig. 3.3g). Analytical error was suspected and a simple dissolution experiment was undertaken to test the results. A 50 g sample of HCl-washed polyminerallic sulphidic mine waste was immersed in 500 ml of 0.01 M H_2O_2 for 24 hours. The leachate was decanted and duplicate samples were submitted to the Cairns Water Laboratory for analysis by turbidometric spectroscopy. The duplicates both returned a concentration of 41 mg/l SO_4^{2-}, which was only slightly higher than the control column leachate results in question (11–29 mg/l), proving the integrity of the latter values.

SEM observations

A summary of the SEM observations (of the waste material removed from the columns at the conclusion of the dissolution stage of the experiment) is presented in Table 3.3. Detailed results and additional SEM micrographs are presented in Appendix B5. The order of phosphate abundance observed in the columns after the dissolution stage was the same as after the coating stage: column D > column C >> column B > column A (based on visual estimations). The amorphous Fe–K–(Cu) phosphate coating (Fig. 3.6a) and the various Pb phosphate phases (Fig. 3.6b) were generally unchanged in appearance and abundance, implying the phases were stable during the dissolution stage. In contrast, the Cu, Zn and Ca phosphate phases were absent from column A material, greatly reduced in abundance in column B and reduced in abundance

in columns C and D, implying their removal during the dissolution stage. Uncommon Ca, Cu, Fe, Pb and Zn sulphates were observed for the first time in Columns A and B. The precipitation of several sulphate crystals onto phosphate phases indicates that these sulphates formed during the experiment. Copper, Fe, Pb and Zn sulphate phases were relatively abundant in the control column waste material.

3.3.5 Discussion

Formation of phosphate phases

The extent of phosphate phase formation in the columns (D > C >> B > A) can be related to the concentration of the oxidant in the coating solution (Table 3.1). Phosphate development in column B was only slightly greater than in column A, though the column B coating solution contained twice the concentration of KH_2PO_4. In addition, phosphate formation in column D (0.2 M H_2O_2) was slightly greater than in column C (0.1 M H_2O_2), even though the column C coating solution contained twice the concentration of KH_2PO_4 than that of column D. This implies that the most important factor controlling phosphate formation under the conditions of the experiment was oxidant strength. This is in agreement with the results of Evangelou (1995b), who found the formation of iron phosphate coating on pyrite to be independent of phosphate in solutions with concentrations as low as 0.0001 M KH_2PO_4. Fytas and Evangelou (1998) reported the optimal coating solution concentrations for forming phosphate coatings on pyritic tailings to be 0.1 M H_2O_2, 0.4 M KH_2PO_4 and 0.2 M NaAC. In addition, Woltmann (2001) found that a concentration of 0.1 M H_2O_2 was required to form phosphate coatings on pure chalcopyrite.

The extent of phosphate development was related to oxidant strength as the H_2O_2 released dissolved cations through the sacrificial oxidation of sulphides (Table 3.4). Most of the reactions listed in Table 3.4 involve the subsequent hydrolysis of the released metal cation to produce a metal hydroxide. In the phosphate coating solution, however, the released metal cation is expected to react with the aqueous phosphate anion, forming a metal phosphate

Table 3.3. Summary of SEM observations of precipitates and coatings found on polymineralic mine waste after the conclusion of the dissolution stage of experiment 1.

Chemistry	Morphology	Abundance
Pb±Ca phosphate (Fig. 3.6b)	pincushions of fine (0.5 µm x 10 µm) acicular crystals, often form extensive coalescences; large (30 µm x 5 µm) tabular crystals, rice-shaped granules and amorphous coatings	pincushions cover >75 % of galena in columns A and B, ~99 % of galena in columns C and D; tabular crystals uncommon precipitates in all columns; granules and coatings observed in columns C and D
Cu-Ca–(K) phosphate (Fig. 3.6a,c)	scattered spherical rosettes of ~10 µm diameter, often form coalescences of radial acicular splays in columns C and D	absent from column A, rare precipitates in column B, cover <10 % of Fe phosphate-coated chalcopyrite surfaces in columns C and D
Fe-K±Cu phosphate (Fig. 3.6a,c)	amorphous coating with extensive desiccation cracks, often layered in columns C and D	thin coating on <1 % of chalcopyrite in column B; thick coating on ~95 % of chalcopyrite, cobaltite and stannite and thin coating on <5 % of pyrite, bournonite and arsenopyrite in columns C and D
Zn-K±Ca phosphate (Fig. 3.6d)	large (100 µm x 10 µm) bladed crystal precipitates; radial flow-like agglomerations of fine-grained (10 µm x 1 µm) acicular crystals	not observed in columns A and B; scattered precipitates in columns C and D; flow-like agglomerations cover <50 % of sphalerite in columns C and D.
Ca±(Si) phosphate	agglomerations of very fine grained (1 µm x 0.1 µm) needles	rare precipitates on <1 % of grains in column B, no preferential substrate.
Pb, Pb-As, Cu, Fe, Zn and Ca sulphates	euhedral rosettes, radial splays, acicular crystals, platelets, blocky prisms and granular precipitates	Ca sulphates cover <1 % of substrate in columns A and B; Pb sulphates common in column A; Pb-As sulphates common in all columns; other sulphates rare precipitates in all columns. Pb and Cu sulphates cover <5 % of mineral grains in the control column

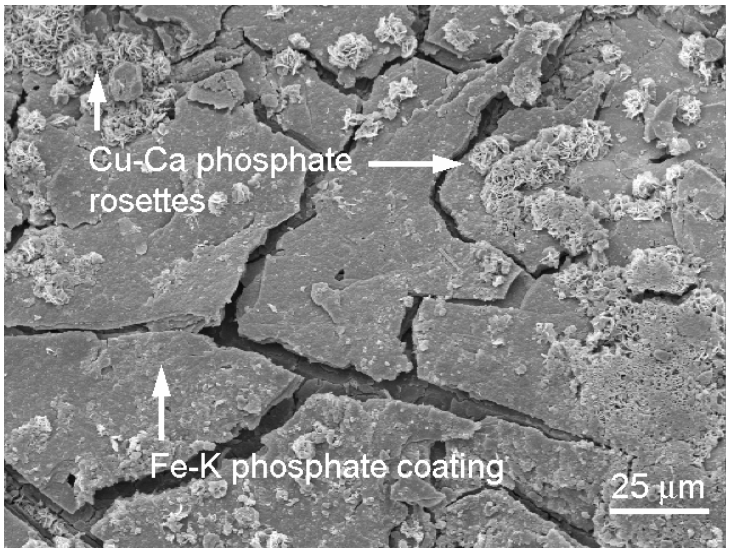

Figure 3.6a.

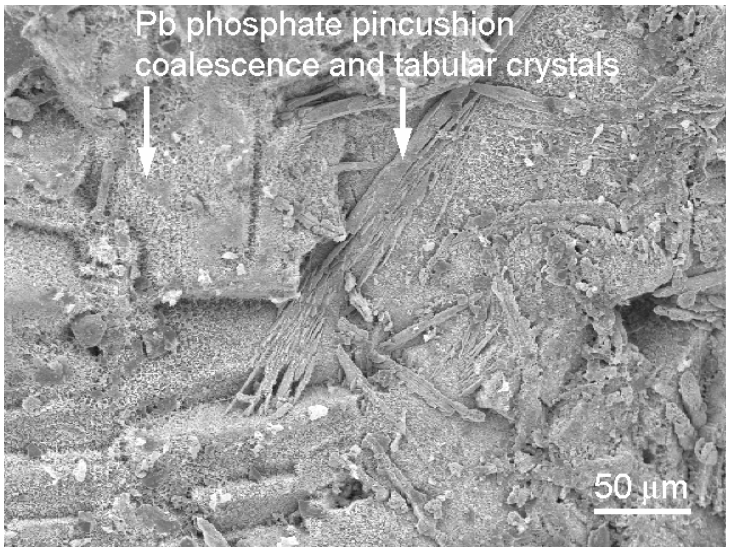

Figure 3.6b.

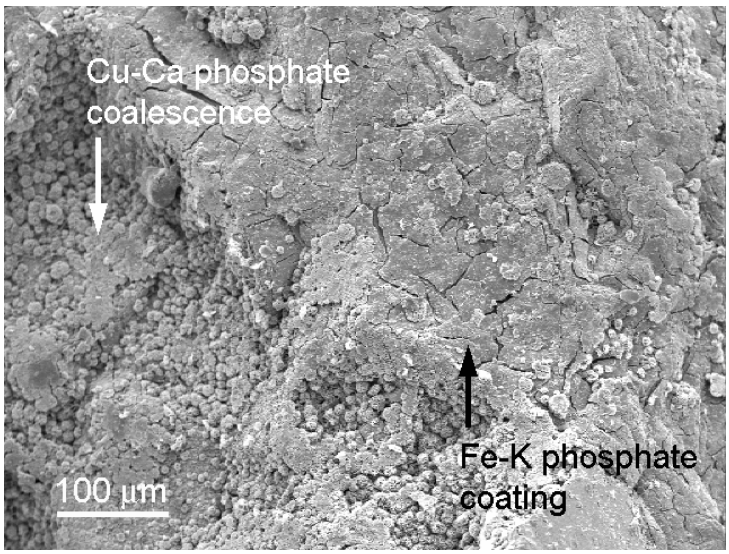

Figure 3.6c.

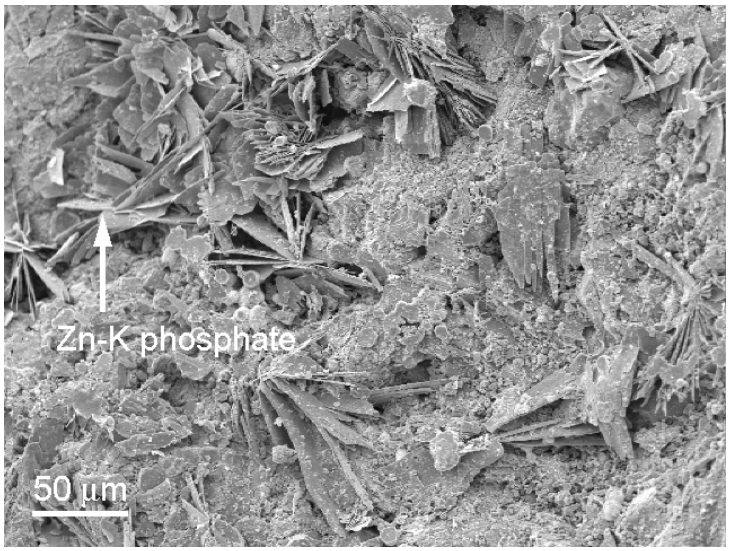

Figure 3.6d.

Figure 3.6. SEM micrographs of material removed from the coated columns after the dissolution stage of experiment 1. a) Fe-K phosphate coating with scattered Cu-Ca phosphate rosettes, column D. b) Pb phosphate pincushions and tabular crystals on galena, column B. c) Fe-K phosphate coating with Cu-Ca phosphate coalescence, column C. d) Bladed Zn-K phosphate crystals, column D.

(Evangelou, 1995a). The reaction for the oxidation of pyrite by H_2O_2 in the presence of phosphate can be described as (Fytas and Evangelou, 1998):

$$FeS_{2(s)} + 7.5H_2O_{2(l)} + H_2PO_4^-{}_{(l)} \rightarrow FePO_{4(s)} + 2SO_4^{2-}{}_{(aq)} + 3H^+{}_{(aq)} + 7H_2O_{(l)} \quad (3.2)$$

The abundance and form of the metal phosphate precipitated is dependent on the degree of saturation of the solution on the mineral surface. A high degree of saturation will lead to the development of a coating on the grain surface, whereas low saturation will cause the precipitation of discrete phases (Evangelou, 1995b). The lower the degree of saturation the coarser the crystals precipitated. The nature and abundance of the phosphate phases observed in the coated columns can therefore be related to leachate chemistry, particularly local saturation of metal $\pm$ alkali phosphate in solutions adjacent to mineral grains.

The near ubiquitous presence and fine-grained nature of the majority of Pb phosphate phases in proximity to galena (Fig. 3.4c; Fig. 3.6b) indicate that the

Table 3.4. Oxidation reactions by H_2O_2 of the major sulphide minerals present in the waste material.

Sulphide	Reaction
arsenopyrite	$FeAsS_{(s)} + 3.5H_2O_{2(l)} + 4H_2O_{(l)} \rightarrow Fe(OH)_{3(s)} + AsO_4^{3-}{}_{(aq)} + SO_4^{2-}{}_{(aq)} + 5H^+{}_{(aq)}$
chalcopyrite	$CuFeS_{2(s)} + 8.5H_2O_{2(l)} \rightarrow Cu(OH)_{2(l)} + Fe(OH)_{3(s)} + 2SO_4^{2-}{}_{(aq)} + 4H_2O_{(l)} + 4H^+{}_{(aq)}$
galena	$PbS_{(s)} + 4H_2O_{2(l)} \rightarrow PbSO_{4(s)} + 4H_2O_{(l)}$
pyrite	$FeS_{2(s)} + 7.5H_2O_{2(l)} \rightarrow Fe(OH)_{3(s)} + 2SO_4^{2-}{}_{(aq)} + 4H^+{}_{(aq)} + 4H_2O_{(l)}$
sphalerite	$ZnS_{(s)} + 4H_2O_{2(l)} \rightarrow Zn(OH)_{2(s)} + 2H_2O_{(l)} + 2H^+{}_{(aq)} + SO_4^{2-}{}_{(aq)}$
tetrahedrite*	$2Cu_3SbS_{3(s)} + 12H_2O_{2(l)} + 4H_2O_{(l)} \rightarrow 6Cu^{2+}{}_{(aq)} + 6SO_4^{2-}{}_{(aq)} + Sb_2O_{4(s)} + 32H^+{}_{(aq)}$ $2Cu_3SbS_{3(s)} + 12H_2O_{2(l)} \rightarrow 6Cu^{2+}{}_{(aq)} + 6SO_4^{2-}{}_{(aq)} + Sb_2O_6^{2-}{}_{(aq)} + 12H^+{}_{(aq)} + 6H_2O_{(l)}$

Equations from Jennings et al., (2000). * The oxidation of tetrahedrite by H_2O_2 has not been reported in the literature. The equations have been adapted from reactions for the oxidation of tetrahedrite by oxygen and water at pH of 3.5 – 8 as suggested by Yakhontova et al., (1980).

degree of saturation of Pb phosphate was high in all columns during the coating stage. Lead phosphates have extremely low solubilities and require low concentrations to achieve saturation (Nriagu, 1983). The abundance of Pb phosphates in all coated columns is a function of this low saturation of formation. The relatively low [Pb] in the coating stage leachates (Fig. 3.3e) can therefore be explained by the ready attenuation of Pb cations into phosphate phases and the resultant prevention of galena oxidation by the Pb phosphate precipitates. A possible reaction for this process is:

$$5PbS_{(s)} + 10.5H_2O_{2(l)} + 3KH_2PO_{4(l)} \rightarrow Pb_5(PO_4)_3OH_{(s)} + 5SO_4^{2-}{}_{(aq)} + 3K^+{}_{(aq)} + 26H^+{}_{(aq)} \qquad (3.3)$$

Reaction 3.3 presumes the precipitated phase to be hydroxypyromorphite, which has been found in phosphate stabilised mine wastes by Eusden et al., (2002). The acicular pincushions observed in the coated columns bear similarity to pyromorphites formed in several experiments which investigated the phosphate stabilisation of Pb in contaminated soils (cf. Lower et al., 1998; Ma et al., 1994; Zhang and Ryan, 1999a). The availability of OH^- in the coating solution, through NaAC addition, coupled with the rapid precipitation of pyromorphite from solutions saturated in pyromorphite (Ma et al., 1993), suggest that the Pb phosphate pincushions are possibly hydroxypyromorphite. However, the SEM/EDS evidence points to the existence of several Pb phosphate phases (additional SEM micrographs in Appendix B5, representative EDS trace in Appendix B8). Identification of the exact stoichiometry of the precipitated phases requires more sensitive surficial analytical methods. The formation of Pb phosphate appeared to be inhibited by the presence of pre-existing anglesite (Fig. 3.7a). This may be due to the low solubility of anglesite precluding the release of Pb ions for complexation with the phosphate anion.

The morphology of the amorphous Fe-K phosphate coatings observed in the coated columns (Fig. 3.4a,b,d; Fig. 3.6a) was very similar to those previously observed on pyrite (cf. Evangelou, 1994; Nyavor and Egiebor, 1995), pyrrhotite (cf. Georgopoulou et al., 1996) and chalcopyrite (cf. Woltmann, 2001). Evangelou (1994) and Georgopoulou et al., (1996) consider the coatings to be $FePO_4$, however they produce no results of any surficial chemical analyses. In contrast, EDS spectra of coated pyrite (Nyavor and Egiebor, 1995) and chalcopyrite (Woltmann, 2001) show the presence of significant K, sourced from the KH_2PO_4 used in the coating solution. The presence of substantial alkalis incorporated into the phosphate coatings observed in the phosphate stabilisation experiments is probably typical of most phosphate coatings formed in previous studies.

The poorly-developed nature of the amorphous Fe-K phosphate coating observed in columns A and B was probably a function of the oxidant concentration. The 0.01 M H_2O_2 used in columns A and B probably did not oxidise chalcopyrite rapidly enough to release sufficient Fe^{2+} to reach iron

phosphate saturation on all chalcopyrite grains. The relationship of the amorphous coating with chalcopyrite suggests the following possible reaction:

$$3CuFeS_{2(s)} + 12H_2O_{2(s)} + 4KH_2PO_{4(l)} \rightarrow$$
$$(Fe^{3+},K)_3(PO_4)_{4(s)} + 3Cu^{2+}{}_{(aq)} + K^{+}{}_{(aq)} + 6SO_4{}^{2-}{}_{(aq)} + 32H^{+}{}_{(aq)} \qquad (3.4)$$

The EDS results indicate minor coprecipitation of Cu^{2+} and Ca^{2+} into the $(Fe,K)_3(PO_4)_4$ crystal lattice (Appendix B8). The formation of $FePO_4$ requires very low activities of Fe^{3+} (Evangelou, 1995b) and is probably thermodynamically and kinetically favoured over $CuPO_4$ formation. This may explain the relative paucity of Cu in the amorphous coatings.

The below detection concentrations (<100 µg/l) of Fe in the coating stage leachates cannot be explained solely by attenuation into the Fe-K phosphate coatings as this phase was uncommon and poorly formed in columns A and B. The formation of ferric hydroxide precipitates is the most likely explanation for the low Fe concentrations as the coating solutions were buffered well above the first hydrolysis constant for iron (pH 2.2) (Nordstrom and Alpers, 1999b). Although Fe-rich precipitates were rarely observed on the grains of waste material, very fine-grained (<1 µm), granular, unidentified precipitates were observed on many sulphide grains when the material was gold-coated (Fig. 3.7b) (the gold coating allows better mineral surface definition at magnifications of >5000x). It is likely that these precipitates were Fe-rich and at least partly responsible for the low [Fe] in the coating stage column leachates.

The paucity of Fe-K phosphate coatings on pyrite (Fig. 3.4a) is contrary to the observations of well-developed coatings on pyrite by Evangelou (1994; 1995b). Pyrite has been observed to generally be more susceptible to oxidation than chalcopyrite (Jambor, 1994) and should therefore form coatings more readily. A possible explanation for the paucity of coating on the pyrite grains is the galvanic protection of pyrite at the expense of chalcopyrite. It has been established in experimental studies that pyrite acts cathodic to many other sulphides, including chalcopyrite, when the minerals are in contact (Peters,

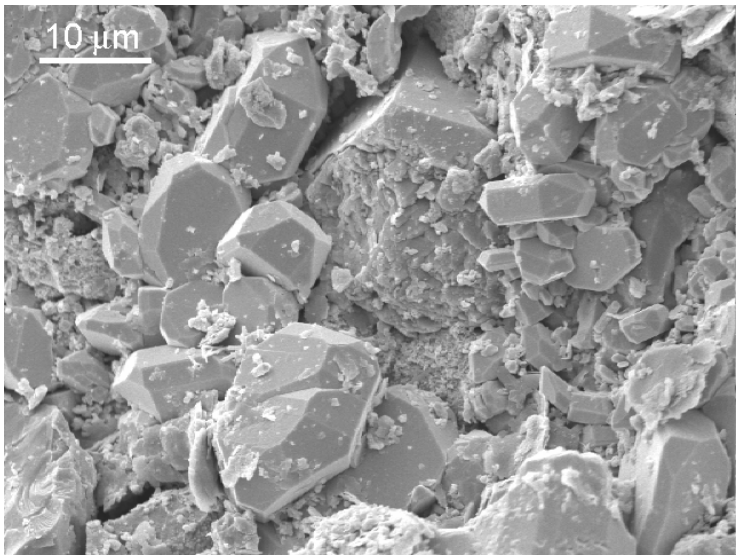

Figure 3.7a.

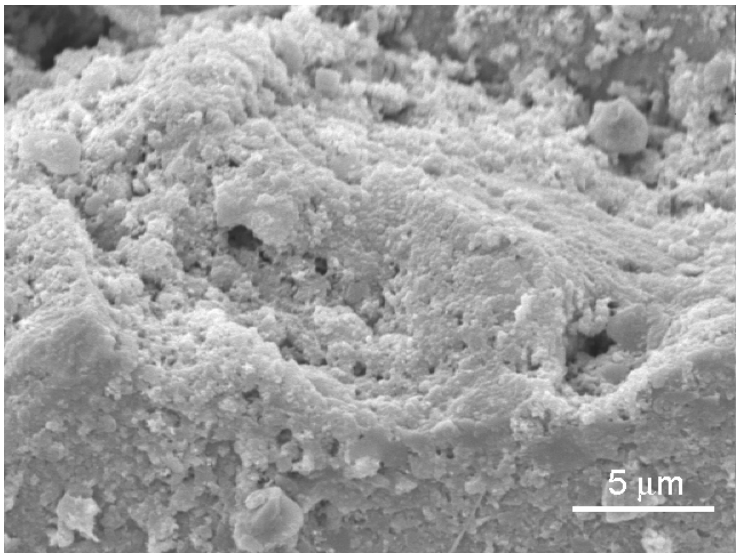

Figure 3.7b.

Figure 3.7. a) SEM micrograph of anglesite crystals which have not reacted with the coating solution, column A. b) SEM micrograph of unidentified granular precipitates on chalcopyrite, possibly Fe (hydr)oxides, column B.

1977; Sato, 1992). This results in accelerated oxidation of the sulphide in contact with pyrite, whilst the pyrite remains relatively unoxidised. This process may have prevented the sacrificial oxidation of pyrite during the coating stage, resulting in a lack of Fe^{3+} to react with phosphate and form coatings.

Cu-Ca phosphates and Zn phosphates were more abundant in columns C and D than in columns A and B. More vigourous oxidation of chalcopyrite and

sphalerite, due to the stronger [H_2O_2], released sufficient Cu^{2+} and Zn^{2+} to attain Cu and Zn phosphate saturation more commonly in columns C and D. This is supported by the observed preferential association of the phosphates with chalcopyrite and sphalerite and also explains the higher [Cu] and [Zn] in the column C and D coating stage leachates (Fig. 3.3c,d). A possible reaction for the formation of the Cu-Ca phosphate rosettes is:

$$3Ca(OH)_{2(l)} + 3Cu^{2+}{}_{(aq)} + 4KH_2PO_{4(l)} \rightarrow (Cu,Ca)_3(PO_4)_{4(s)} + 4K^{+}{}_{(aq)} + 2H^{+}{}_{(aq)} + 6H_2O_{(l)} \quad (3.5)$$

The Cu^{2+} is sourced from Reaction 3.4. Higher [Cu^{2+}] near chalcopyrite surfaces allowed the precipitation of fine-grained rosettes, whereas on other minerals, lower [Cu^{2+}] led to the formation of isolated, coarser precipitates. Areas in proximity to sphalerite grains in columns C and D had [Zn^{2+}] high enough to permit formation of fine-grained precipitates of Zn-K phosphate (Fig. 3.4b) (representative EDS trace in Appendix B8). Late precipitates of identical chemistry were coarser-grained due to lower [Zn^{2+}]. A possible reaction for this process is:

$$ZnS_{(s)} + 2H_2O_{2(l)} + KH_2PO_{4(l)} \rightarrow (Zn,K)PO_{4(s)} + SO_4{}^{2-}{}_{(aq)} + 6H^{+}{}_{(aq)} \quad (3.6)$$

Isolated precipitates of Zn phosphate tended to contain Ca rather than K, implying late precipitation after the addition of $Ca(OH)_2$:

$$3ZnS_{(s)} + 3Ca(OH)_{2(l)} + 3H_2O_{2(l)} + 4KH_2PO_{4(l)} \rightarrow (Zn,Ca)_3(PO_4)_{4(s)} + 3SO_4{}^{2-}{}_{(aq)} + 4K^{+}{}_{(aq)} + 20H^{+}{}_{(aq)} \quad (3.7)$$

The ubiquitous presence of Ca in the Cu-Ca phosphate rosettes suggests that the rosettes did not form until the addition of $Ca(OH)_2$ and the resultant pH rise at the end of the coating stage. It is probable, however, that with $Ca(OH)_2$ addition a layer of Cu-Ca phosphate precipitated on pre-existing Cu phosphate crystals. Inspection of coated column material prior to the addition of $Ca(OH)_2$ is required to ascertain if this has occurred.

Tetrahedrite showed an absence of phosphate coatings and a paucity of Cu-Ca phosphate rosettes. The poor phosphate development cannot be explained by slow oxidation and little resultant cation release as the high coating stage leachate [Sb], particularly in columns C and D (Fig. 3.3b), indicate that significant tetrahedrite oxidation occurred. In addition, the few studies published on tetrahedrite oxidation state that it has a similar reactivity to chalcopyrite (Yakhontova et al., 1980) or is more susceptible to oxidation than chalcopyrite (Boyle, 1994; Brock, 1979). Iron phosphate coatings were not formed because tetrahedrite lacks Fe. Dissolved Sb most likely existed as SbO_3^- within the columns (Vink, 1996), which would not react with phosphate anions and should be relatively mobile at pH 5–6. This explains the lack of Sb phosphates and the high [Sb] in the coating stage leachates. It is unclear why Cu phosphate rosettes did not form abundantly on tetrahedrite as appreciable Cu^{2+} should have been released by tetrahedrite oxidation (Table 3.4) (Yakhontova et al., 1980). The paucity of phosphates on tetrahedrite is not due to a lack of phosphate, as the presence of Ca phosphate crystals in all columns indicates that PO_4^{3-} remained available at the conclusion of the coating stage.

The concentrations of As in the coating stage leachates decreased steadily but significantly during the coating stage (Fig. 3.3a). This indicates depletion of the source of the As. The oxidation of arsenopyrite and arsenian tetrahedrite are the most likely sources of As. The oxidation of arsenopyrite may have been partially inhibited by the formation of minor phosphate coatings during the coating stage, particularly in columns C and D. The attenuation of As by Pb-As sulphate precipitation would have also removed small quantities of As from solution.

The SO_4^{2-} concentrations in the coating stage leachates are probably a function of SO_4^{2-} release through sulphide oxidation, dissolution of sulphates which survived the HCl washing and desorption from iron (hydr)oxides (Rose and Elliot, 2000; Rose and Ghazi, 1997). The decrease in leachate SO_4^{2-} concentrations during the coating stage (Fig. 3.3g) is probably due to flushing of mobile aqueous SO_4^{2-} out of the columns, depletion of soluble sulphate

minerals with continuing dissolution and inhibition of sulphide oxidation as a result of the formation of phosphate coatings.

The abundance, location and morphology of phosphates formed during the coating stage were controlled by the level of saturation of the metal ± alkali phosphate in the solution adjacent to mineral grains. The major factor controlling the level of saturation was the coating solution oxidant strength and subsequent cation release from sacrificial sulphide oxidation. Sulphide oxidation also had an important affect on the leachate dissolved element concentrations. Several other factors, such as the precipitation of iron (hydr)oxides, sorption/desorption reactions of elements with secondary mineral surfaces and the kinetics of all of the above processes may also have had a significant effect on the leachate chemistry.

Stability of phosphate phases

The order of abundance of phosphate phases observed in the coated columns after the conclusion of the dissolution stage matched the order of final pH in the dissolution stage leachate (column D > column C >> column B > column A) (Fig. 3.5a). This indicates that the extent of phosphate coating development controls the pH through the inhibition of sulphide oxidation, particularly the amorphous Fe-K phosphate coatings on chalcopyrite. The stability of the amorphous Fe-K phosphate coatings was demonstrated by their persistence through the dissolution stage (Fig. 3.6a,c), even when poorly-developed as in columns A and B. The formation of an impervious phosphate coating on the sulphides, particularly chalcopyrite, prevented the oxidant from accessing the sulphide surface, halting oxidation (Evangelou, 1995b).

Unlike the pH, the [Fe] in the dissolution stage leachates was not controlled by the amorphous Fe-K phosphate coatings as [Fe] was similar in all column leachates, including the control (Fig. 3.3f). The low [Fe] in the control column leachates throughout the majority of the dissolution stage was possibly a result of attenuation by iron (hydr)oxide precipitation through rapid hydrolysis of Fe^{3+} at pH values above the first hydrolysis constant of iron (Nordstrom and Alpers,

1999b). The increased [Fe] in the coated column dissolution stage leachates was possibly a result of the iron precipitates formed during the coating stage becoming unstable at the alkaline pH caused by the addition of $Ca(OH)_2$.

The stability of the Pb phosphates was also demonstrated by their persistence in all columns after the dissolution stage (Fig. 3.6b). The Pb phosphates probably inhibited galena oxidation, reflected in the very low coated column dissolution stage leachate [Pb] as compared with the control column leachate [Pb] (Fig. 3.3e). The jump in coated column leachate Pb concentration at the start of the dissolution stage is probably a result of mobilisation of Pb^{2+} as a function of the pH rise through the $Ca(OH)_2$ addition. The specific process responsible for this increase in mobility is unknown.

The reduced abundance of Cu-Ca phosphate rosettes and Zn phosphates in all coated columns after the dissolution stage indicates these phase were relatively unstable in the oxidising solution. Dissolution of these phosphates probably explains the steady rise in [Cu] and [Zn] in the coated column leachates during the dissolution stage (Fig. 3.3c,d). Despite the phosphate dissolution, concentrations of Cu and Zn in the coated column leachates remained well below concentrations of Cu and Zn in the control column leachates throughout the dissolution stage. With decreasing pH in the coated column leachates the solubility of the Zn phosphate phases may have increased, resulting in greater Zn release (Fig. 3.3d). The relatively high [Zn] in the column A dissolution stage leachates is probably also a reflection of increased sphalerite oxidation due to reduced inhibition from Zn phosphate precipitates.

The ability of the metal $\pm$ alkali phosphates to reduce dissolved metal concentrations in the coated column leachates, particularly Pb, is in agreement with previous phosphate stabilisation studies of mine waste (cf. Eusden et al., 2002) and metal contaminated soils (cf. Cotter-Howells and Caporn, 1996; Ruby et al., 1994). It is possible that the reduced base metal concentrations in the coated column leachates merely reflects reduced mobility at higher pH. Further experiments are required to solve this issue by using a control column which has added $Ca(OH)_2$ to raise the pH but no added phosphate.

The initial very high Cu and Pb concentrations in the control column leachates (Fig. 3.3c,e) were probably due to flushing of metals mobilised through the dissolution of remnant sulphates and desorption from mineral surfaces at low pH (3.48). After depletion of the readily mobilised Cu and Pb, the concentrations in the control column leachates stabilised, controlled by chalcopyrite and galena oxidation. In contrast, there was no initial [Zn] peak in the control column leachates (Fig 3.3d). This may indicate that all readily mobilised Zn was removed from the control column by the HCl wash and sphalerite oxidation controlled the [Zn] in the control column leachates from the start of the dissolution stage.

The presence of fine-grained Cu, Fe, Pb, Pb-As and Zn sulphates precipitated on phosphate phases in the coated columns indicates that some sulphate formation occurred during the experiment. The major source of the sulphate anion was probably the oxidation of sulphides, as the sulphate phases were abundant in the control column and more common in column A and B than in column C and D. However, the similar [SO_4^{2-}] in the control and coated column leachates is problematic as sulphide oxidation, and therefore SO_4^{2-} release, should have been much greater in the control column than the coated columns. Control column leachate SO_4^{2-} was possibly attenuated by metal/alkali sulphate precipitation and adsorption of SO_4^{2-} onto iron (hydr)oxides (Rose and Elliot, 2000; Rose and Ghazi, 1997). However, given that metal concentrations in the control column leachates were far greater than in the coated column leachates and Fe-rich precipitates were not observed in abundance in the control column material, it seems unlikely that these processes could have removed sufficient SO_4^{2-} to reduce the control column [SO_4^{2-}] to the values measured. Further work is required to ascertain the behaviour of SO_4^{2-} in the control column leachates.

The concentrations of As and Sb were consistently higher in the coated column dissolution stage leachates than in the control column leachates (Fig. 3.3a,b). This was probably related to the greater mobility of these elements in the higher pH of the coated column leachates. The low metalloid concentrations in the control column dissolution stage leachates were possibly due to As and Sb

attenuation by ferric precipitates in acidic solutions. Arsenic may also have been removed from solution by the precipitation of Pb-As sulphates in the control column. Substantial mobilisation of the metalloids, particularly Sb, occurred with the addition of $Ca(OH)_2$ and the resultant rise in pH (Fig. 3.3a,b). Flushing and depletion of the readily mobilised As and Sb led to the stabilisation of the concentrations at values probably controlled by the oxidation of tetrahedrite and arsenopyrite. The higher pH values of the coated column leachates prevented As and Sb attenuation and the metalloids remained in solution.

The relative stabilities of the phosphate phases formed during the coating stage had an important control on the coated column leachate chemistry during the dissolution stage. The persistence of the amorphous Fe-K phosphate coatings inhibited oxidation and subsequent acid generation in columns C and D. The stability of the Pb phosphates resulted in low [Pb] in all column leachates throughout the dissolution stage. The Cu and Zn phosphates were less stable in the oxidising solution and concentrations of Cu and Zn rose during the dissolution stage due to the dissolution of these phases. The concentrations of As and Sb during the dissolution stage were higher in the coated column leachates due to their greater mobility at the relatively high leachate pH and the lack of phosphate coating on tetrahedrite, which allowed oxidation to proceed.

3.3.6 Limitations specific to experiment 1

The HCl washing of the polyminerallic sulphidic mine waste was intended to remove all soluble secondary phases from the columns, retaining only pure sulphides and quartz. However, SEM observation of HCl-washed grains identified the presence of remnant secondary minerals, mainly the sparingly-soluble Pb sulphate anglesite, but also unidentified Cu and Fe sulphates. The contribution the continued dissolution of these remnant sulphates made to the column leachate chemistry is unknown. In addition, traces of iron (hydr)oxides were also present in the mine waste after the HCl wash. The effects these phases had on the column leachate chemistry, particularly through sorption/desorption reactions, is also unknown.

3.3.7 Summary

The results of the experiment showed that phosphate coatings could be formed to some extent on polymineralllic, sulphidic waste material. The extent and morphology of phosphate species formed was dependent on the concentration of oxidant used in the coating solution rather than the phosphate concentration. The concentration of 0.01 M H_2O_2 used in columns A and B was insufficient to release enough metal ions to form extensive coatings or coalescences on any sulphide minerals except galena. The low saturation levels of Fe, Cu and Zn phosphate only permitted the formation of discrete, isolated metal phosphate crystals and occasional, poorly-developed coatings in columns A and B. The increased oxidant concentration in the column C and D coating solutions allowed greater oxidation of chalcopyrite and subsequent saturation of Fe-K phosphate to occur. This resulted in an amorphous coating forming on practically all chalcopyrite surfaces. This coating was the most effective in inhibiting oxidation and acid generation in the dissolution stage of the experiment.

The phosphate precipitates probably also inhibited the release of Pb and, to a lesser extent, Cu and Zn into solution. However, the reduced base metal concentrations in the coated column leachates may have been due to the elevated pH alone. Fe concentrations were also attenuated in all columns, however, the below detection [Fe] of the control leachates indicate that another process, such as ferric hydroxide precipitation, was inhibiting Fe release. Arsenic and Sb did not form phosphate phases and their release was not inhibited in the coated column dissolution stage leachates. Further work is required to investigate the effects of $Ca(OH)_2$ addition on the formation of phosphates and their ability to inhibit acid generation and attenuation of dissolved metals.

3.4 Phosphate stabilisation of partly oxidised, polyminerallic mine waste using liquid chemical stabilisers (experiment 2)

3.4.1 Aims

Experiment 1 demonstrated the ability of the phosphate stabilisation technique to form oxidation inhibiting, metal attenuating phosphate phases on polyminerallic, unoxidised, sulphidic mine waste. The samples used in experiment 1 were HCl washed to remove any soluble phases and therefore do not represent actual mine waste characteristics, especially at abandoned historic mine sites. In contrast, experiment 2 used partly oxidised mine waste to investigate the effect of abundant secondary phases on the phosphate stabilisation technique.

The specific aims of experiment 2 were:

a) to determine the morphologies and chemistries of any phosphate phases formed by the interaction of partly oxidised, polyminerallic mine waste with liquid phosphate stabilisers;

b) to determine the stability, metal attenuation ability and acid generation inhibition ability of any phosphate phases formed by the interaction of partly oxidised, polyminerallic mine waste with liquid phosphate stabilisers.

3.4.2 Specific methodology

The waste material used in experiment 2 was sourced from homogenised, quartered, composite mine waste samples collected from waste dump faces of the abandoned Montalbion silver mine (Chapter 2). In contrast to experiment 1, the waste material was not washed with HCl in order to retain the soluble secondary minerals. The XRD and bulk XRF results for the partly oxidised, polyminerallic waste material used in the columns of experiment 2 are tabulated in Appendix B1. The porosity of the material was considered adequate to

ensure saturation of the entire column. Therefore, 400 g of waste material was placed into each column without any additional quartz sand.

The compositions and concentrations of the coating solutions used in experiment 2 were identical to those used in experiment 1 (Table 3.5).

Table 3.5. Coating solutions used in the coating stage of experiment 2.

	Oxidant	Phosphate	Buffer
Column A	0.01 M H_2O_2	0.2 M KH_2PO_4	0.2 M CH_3COONa
Column B	0.01 M H_2O_2	0.4 M KH_2PO_4	0.2 M CH_3COONa
Column C	0.1 M H_2O_2	0.4 M KH_2PO_4	0.2 M CH_3COONa
Column D	0.2 M H_2O_2	0.2 M KH_2PO_4	0.2 M CH_3COONa

Five litres of coating solution were added to the respective columns at a rate of 400 ml per day. During the coating stage, leachate samples were collected after the addition of 400 ml, 2600 ml and 5000 ml of coating solution. These samples were analysed for As (0.5 mg/l), Cu (0.1 mg/l), Fe (0.1 mg/l), Pb (0.7 mg/l), S (1 mg/l), Sb (0.08 mg/l), and Zn (0.05 mg/l) by ICP-AES. Detection limits are shown in brackets.

The dissolution stage of the experiment consisted of the addition of 5000 ml of 0.01 M H_2O_2 at a rate of 400 ml per day. Leachate samples were collected after the addition of 200 ml, 800 ml, 1600 ml, 2000 ml and then every 600 ml addition until the addition of 5000 ml of oxidant. These samples were analysed for Al (100 µg/l), As (1 µg/l), Cu (0.1 µg/l), Pb (0.5 µg/l), Sb (0.1 µg/l) and Zn (5 µg/l) by ICP–MS and for Fe (0.1 mg/l) and S (1 mg/l) by ICP-AES. Detection levels are shown in brackets.

Samples of waste material were removed from the columns at the completion of the coating and dissolution stages. In addition, further aliquots of waste material (~30 g) were removed from each column after the addition of 5000 ml of coating solution but prior to the addition of $Ca(OH)_2$. These samples were prepared for

SEM observation and EDS analysis (Section 3.2.3) in order to determine whether the addition of $Ca(OH)_2$ was required to precipitate phosphate phases.

3.4.3 Coating stage results

Coating stage leachates initially contained small quantities of light brown precipitates, which were probably partly disassociated Fe compounds and slightly soluble sulphates. The leachates became clear after the addition of approximately 2000 ml of coating solution. Complete chemical results for the coating stage leachates are tabulated in Appendix B3.

Leachate chemistry

Coating solutions were buffered to pH 5.2–5.8 for the duration of the coating stage (Fig. 3.8a). The pH of all columns increased steadily with coating solution addition due to instrumental drift. Recalibration of the pH meter resulted in a pH drop, however, the instrumental drift continued. The electrode was replaced at the conclusion of the coating stage to solve the problem. Despite the instrumental drift, pH drift for individual columns for the duration of the coating stage was restricted to 0.4 of a pH unit. Instrumental problems caused 0.2 pH units of that drift, indicating that pH drift for each column was limited to 0.2 pH units during the coating stage (Fig. 3.8a). The pH of column A and D leachates were higher than column B and C leachates, generally by 0.2 pH units, due to the greater concentration of KH_2PO_4 in column B and C coating solutions (Section 3.3.3).

The conductivities of the coating stage leachates were very high due to the KH_2PO_4 and NaAC used in the coating solutions (20 000 µS/cm – 70 000 µS/cm) (Fig. 3.8b). Although the conductivities rose and fell inexplicably during the coating stage, the values of column B and C leachates were always greater than the conductivities for leachates from columns A and D, due to the stronger KH_2PO_4 concentrations of the column B and C coating solutions (Table 3.5).

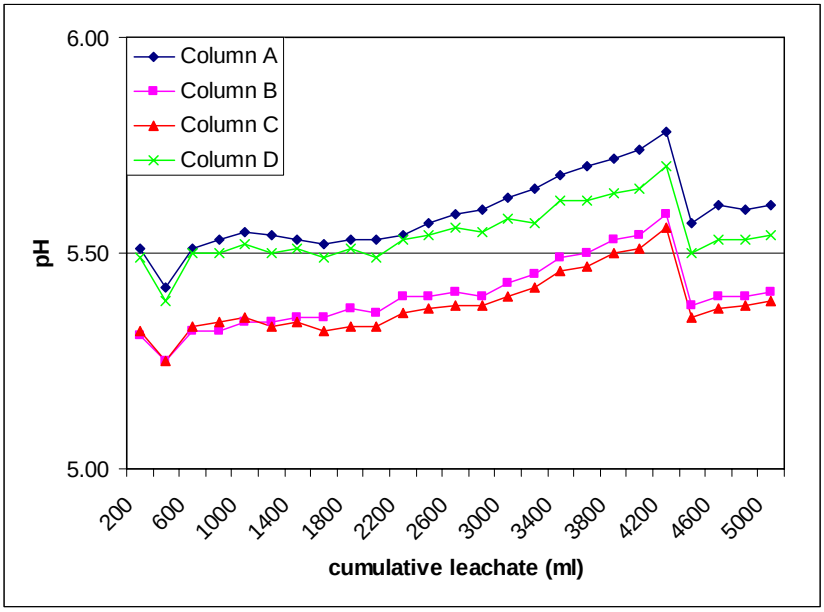

Figure 3.8a.

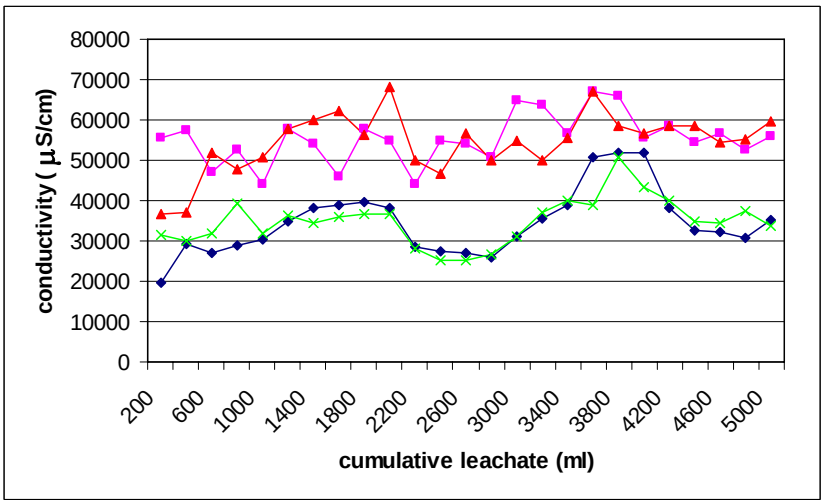

Figure 3.8b.

Figure 3.8. Experiment 2 pH (a) and conductivity (b) of coating stage leachates. Legend for (a) also applies to (b).

As in experiment 1, the coating stage leachate [Fe] was below detection in all columns. Concentrations of As, Cu, SO_4^{2-} and Zn dropped during the coating stage by 93 %, 75 %, 73 % and 51 % respectively (average of the four columns) (Fig. 3.9). In contrast to experiment 1 however, [Pb] dropped or rose slightly and [Sb] rose by 60 % during the coating stage (average of the four columns) (Fig. 3.9b,g). The overall elemental abundance in the coating stage column leachates (average of the four columns' cumulative element release

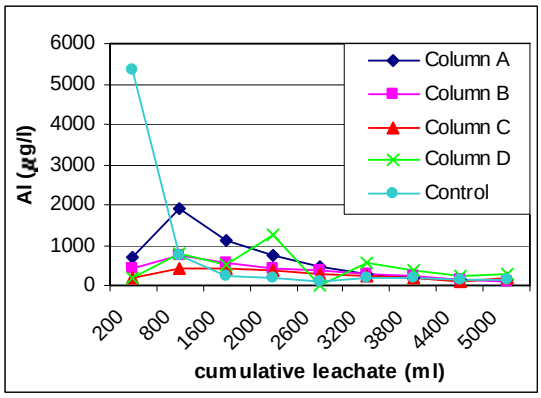

Figure 3.9a. Al

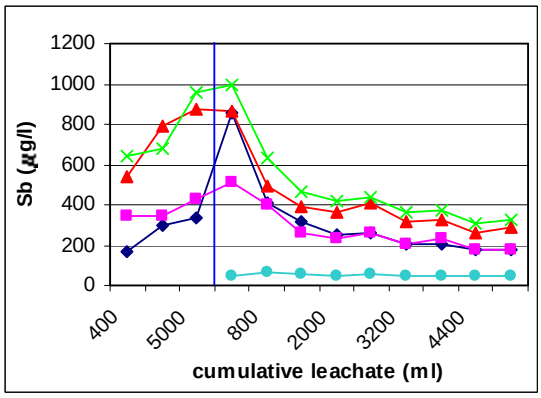

Figure 3.9b. Sb

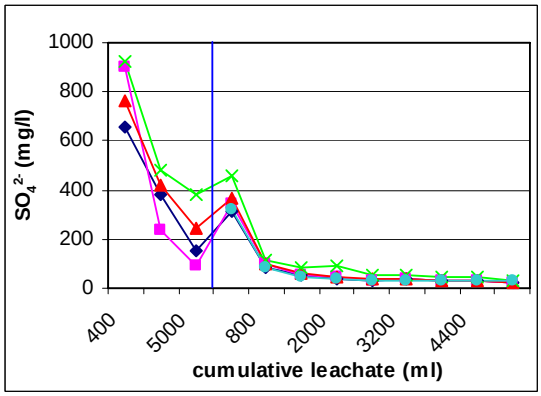

Figure 3.9c. SO_4^{2-}

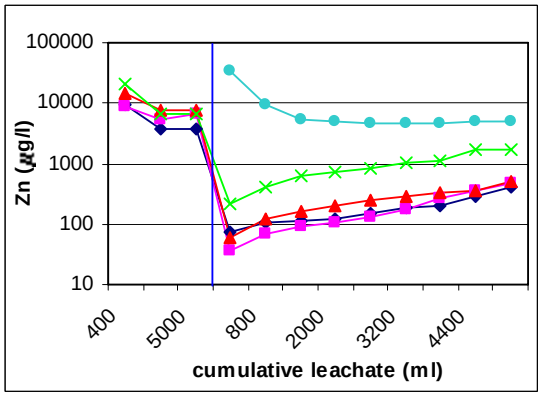

Figure 3.9d. Zn

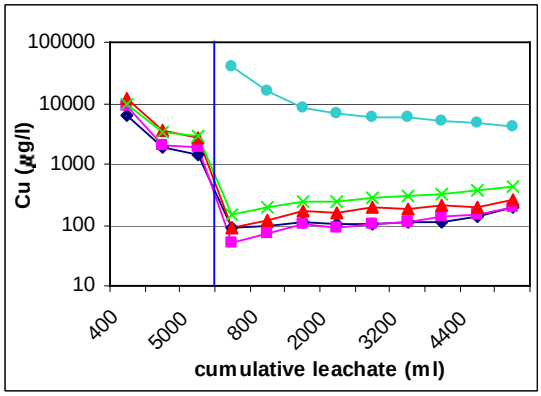

Figure 3.9e. Cu

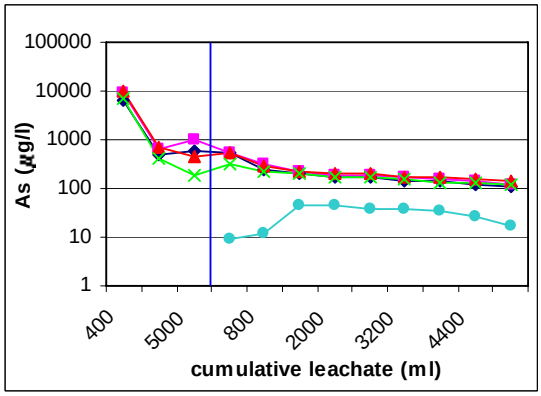

Figure 3.9f. As

Figure 3.9. Concentrations of elements in leachates of experiment 2. Legends for (a) and (h) are applicable to all graphs. Vertical line represents addition of $Ca(OH)_2$ and separates coating stage results (left of the line) from dissolution stage results (right of the line). Leachates were not analysed for Al in the coating stage.

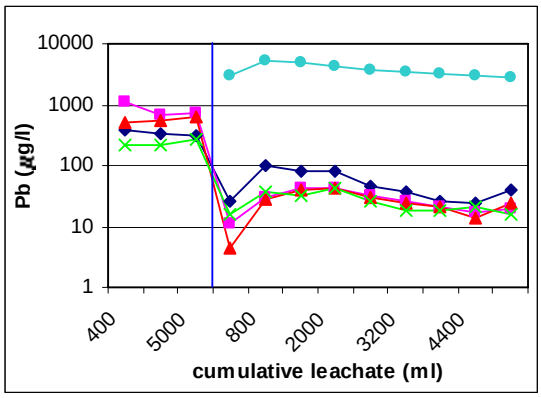

Figure 3.9g. Pb

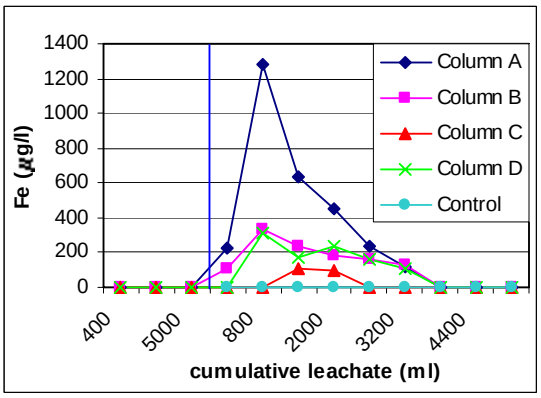

Figure 3.9h. Fe

Figure 3.9. (continued)

during the coating stage) was SO_4^{2-} > Zn > Cu > As > Sb > Pb > Fe, which was similar to experiment 1. The absolute cumulative quantities of coating stage leachate SO_4^{2-}, Pb and Zn were higher in experiment 2 than in experiment 1, whereas quantities of As, Cu and Sb were lower then experiment 1 coating stage leachates.

The order of elemental abundance in the bulk XRF results of the partly oxidised, polyminerallic waste was Si > S > Pb > Al > Fe > Cu > Zn > Sb > As (Appendix B1). Comparing this to the order of elemental abundance in the coating stage leachates highlights the relative immobility of Pb and Fe and the mobility of As, Cu and Zn in the coating stage leachates.

SEM observations

A summary of the SEM observations (on the material removed from the coated columns prior to $Ca(OH)_2$ addition) is presented in Table 3.6. Detailed results and additional SEM micrographs are presented in Appendix B6. Abundant phosphate phases were observed in material removed from all the coated columns prior to $Ca(OH)_2$ addition (Fig. 3.10), which demonstrates that the $Ca(OH)_2$ stabiliser was not required to form phosphate coatings or precipitates.

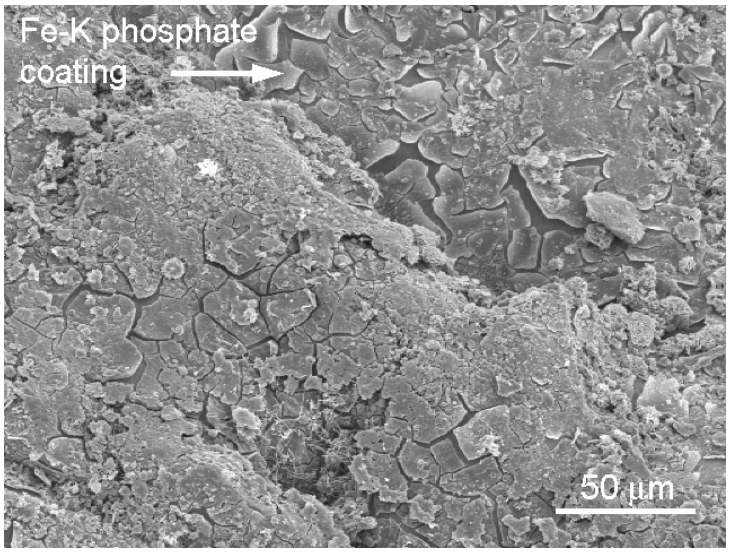

Figure 3.10a.

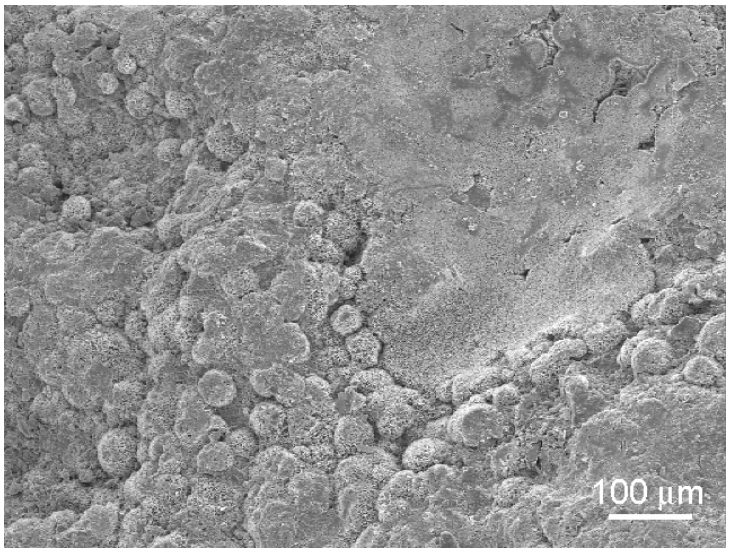

Figure 3.10b.

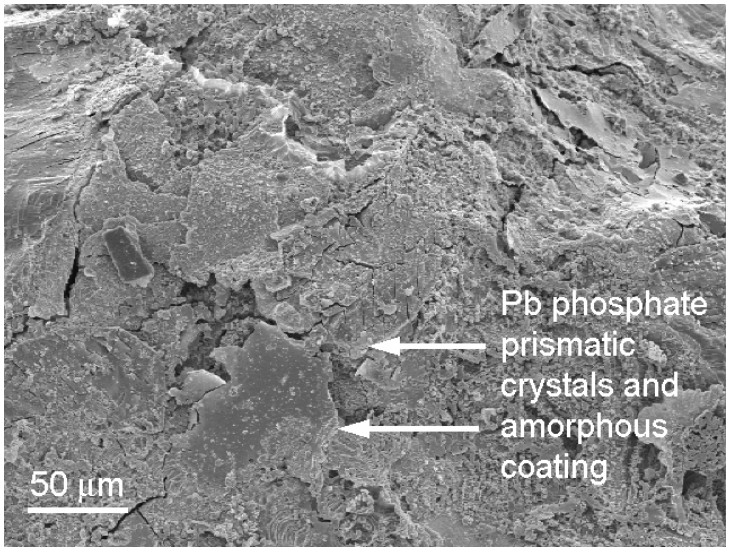

Figure 3.10c.

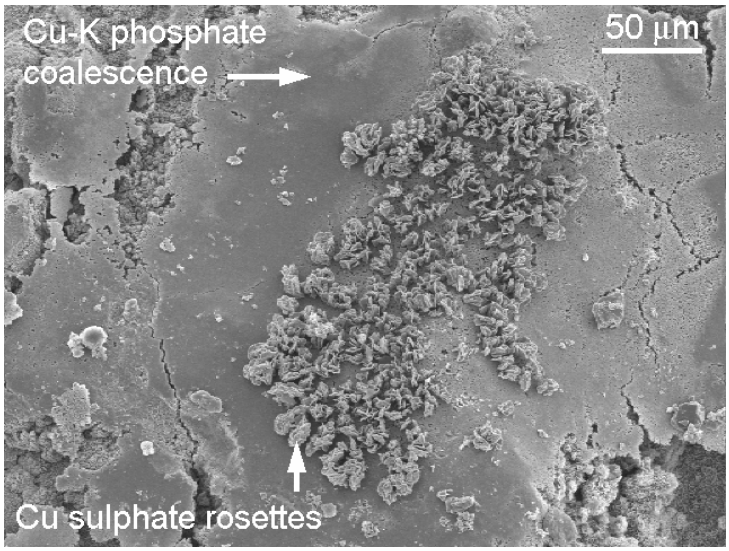

Figure 3.10d.

Figure 3.10. SEM micrographs of material removed from the coated columns after the coating stage of experiment 2 and pre-$Ca(OH)_2$ addition. a) Thin, poorly-developed Fe-K phosphate coating on chalcopyrite, column A. b) Cu-K phosphate coalescence, column A, EDS trace in Appendix B8. c) Amorphous coating and crystals of Pb phosphate, column D. d) Cu sulphate crystals precipitated on Cu-K phosphate coalescence, column D.

The overall order of extent of phosphate formation was the same as in experiment 1; column D > column C >> column B > column A. This did not apply to all phosphate phases, for example, Zn phosphates were more abundant in column C than in column D. Phosphate phases were more abundant than those observed after the coating stage in experiment 1, particularly in columns A and B (Fig. 3.10a,b). The same major forms of phosphate phase were observed as in experiment 1 (i.e. Fe-K±Cu phosphate coatings and metal ± alkali phosphate crystal precipitates), however, greater variety in chemistry and morphology was observed. Amorphous Fe-K phosphate coatings were most extensively developed on chalcopyrite (Fig. 3.10a). These coatings were also occasionally observed on sphalerite and tetrahedrite, which were uncoated in experiment 1. Significant quantities of Zn and S were also detected in the amorphous coatings.

The interaction of the coating solution with the secondary phases present in the waste material seemed to be dependent on the solubility of the secondary mineral. Sulphate minerals with low solubilities, such as anglesite, plumbojarosite, beaverite and osarizawaite had only occasional, poorly-formed

Table 3.6. Summary of SEM observations of precipitates and coatings formed on partly oxidised polyminerallic mine waste in columns during the coating stage of experiment 2, prior to the addition of $Ca(OH)_2$.

Chemistry	Morphology	Abundance
Pb±K phosphate (Fig. 3.10c)	extensive coalescences of pincushions of fine (0.5 µm x 10 µm) acicular crystals; large (30 µm x 10 µm) bladed and leafy crystals and amorphous to scaly coatings	pincushions cover ~99 % of galena in all columns, large crystals cover ~10 % of galena in column D, rare precipitates in other columns; coatings rare in column D
Cu-K±(Si, Fe, S, Al) phosphate (Fig. 3.10b,d)	scattered spherical rosettes up to 30 µm diameter, often form coalescences of radial acicular splays	heterogeneous development, cover 100% of some grains, absent on others; abundant on coated chalcopyrite, scattered on quartz, clays, tetrahedrite and oxides
Fe-K±(Cu-Zn-S) phosphate (Fig. 3.10a)	amorphous coating with extensive desiccation cracks, variable thickness	thin coating on ~75 % of chalcopyrite in column A and B; thick coating on ~99 % of chalcopyrite and stannite and thin coating on 99 % of arsenopyrite in columns C and D; sphalerite and tetrahedrite rarely coated in columns A, B and D
Zn-K±(S) phosphate (Appendix B6)	large (200 µm x 100 µm) prismatic crystals; radial flow-like agglomerations of fine-grained (10 µm x 1 µm) acicular crystals; amorphous spheroids	large crystals and amorphous spheroids scattered precipitates in all columns; flow-like agglomerations cover ~40 % of sphalerite in columns C and D.
Pb, Cu, Fe sulphates (Fig. 3.10d)	euhedral rosettes, botryoids, fibres and blocky prisms	Cu sulphates rare isolated precipitates in columns A, B and C, occasionally extensive in column D; Pb and Fe sulphates rare precipitates in columns C and D

phosphates precipitated on them. Copper and Fe sulphates, presumably with high solubilities, usually had extensive phosphate precipitates on them. Iron oxides observed in the waste material also had only rare and poorly-formed

precipitates of phosphate on them. A greater abundance and variety of sulphate phases (Cu, Fe and Pb sulphates) were precipitated on phosphate phases during experiment 2 than in experiment 1 (Fig. 3.10d).

Detailed results of the SEM observations of the material removed from the coated columns after the addition of $Ca(OH)_2$ are tabulated in Appendix B6. The addition of $Ca(OH)_2$ increased the chemical and morphological variation of phosphate phases observed in the coated column material (Appendix B6). However, the absolute abundance of phosphate appeared unaffected by the addition of $Ca(OH)_2$. The exception was Zn phosphate, which appeared to be less abundant in column A and D after $Ca(OH)_2$ addition. This may be a reflection of the limited sample size coupled with the heterogeneity of Zn phosphate development. The addition of $Ca(OH)_2$ resulted in the formation of metal – Ca±K phosphates (Fig. 3.11a), either through the precipitation of discrete metal–Ca phases or the incorporation of Ca into pre-existing metal–K phosphates. Scattered Ca phosphate precipitates were also observed in columns A, B and C. The addition of $Ca(OH)_2$ to the columns had no affect on the chemistry, morphology and abundances of sulphates (Fig. 3.11b) except for the added presence of rare Ca±K sulphates in columns A and B and rare Pb–Ca–K sulphates in column B.

The Cu-K±Ca phosphate rosettes often formed coalescences over entire grains too thick and well-developed to allow determination of the substrate, even in columns A and B where rosette development on chalcopyrite was relatively poor (Fig. 3.11b). In an attempt to determine the substrate for these well-developed rosette coalescences, two previously observed, well-coated grains, removed from columns B and A prior to- and post-$Ca(OH)_2$ addition respectively, were removed from their SEM stubs. The phosphate coating was carefully removed with a razor blade and the grains were placed on stubs for SEM/EDS observation and analysis. In all instances the substrate proved to be a blue Cu sulphate, possibly chalcanthite.

Large crystals of Cu, Zn and Pb phosphate were removed from well-coated grains taken from column D after the coating stage. The crystals were then

analysed by general area detector diffraction system (GADDS) at JCU AAC, Townsville. The best match for the diffraction patterns were produced by $Cu_4H(PO_4)_3.3H_2O$ (powder diffraction file (pdf) No. 49-1145), $KZnPO_4$ (pdf No. 34-0194) and a mix of $Pb_5(PO_4)_3OH$ (pdf No. 08-0259) and $PbHPO_4$ (pdf No. 29-0773). GADDS traces of the Zn and Pb phosphate phases are presented in Appendix B8. None of these phases have a natural analogue.

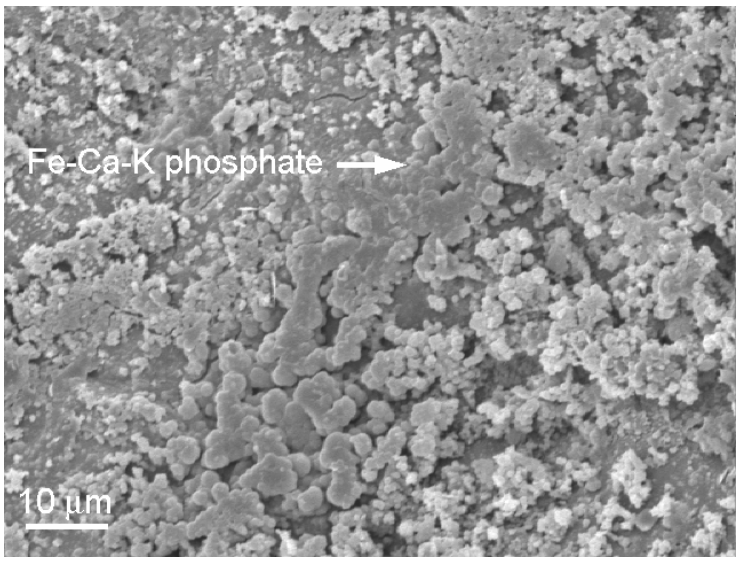

Figure 3.11a.

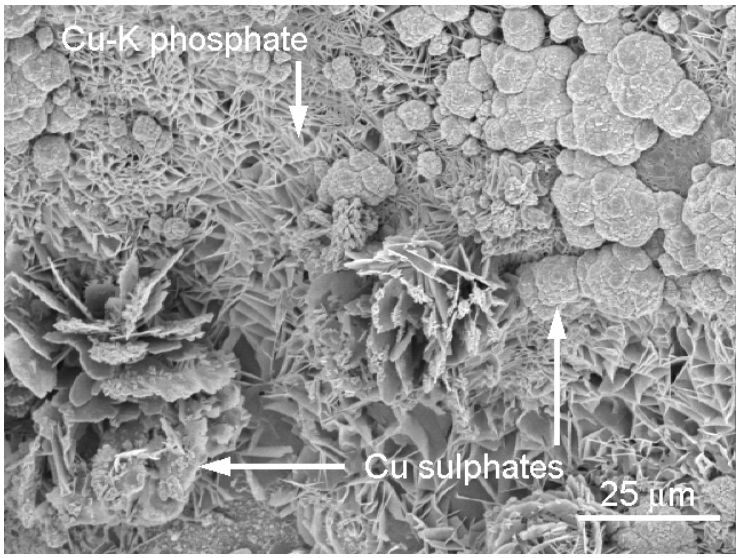

Figure 3.11b.

Figure 3.11. SEM micrographs of material removed from the coated columns after the coating stage and post-$Ca(OH)_2$ addition. a) Granular Fe-Ca-K phosphate on chalcopyrite, column B. b) Rosettes and botryoids of Cu sulphate on Cu-K phosphate coalescence, column B.

3.4.4 Dissolution stage results

Leachate chemistry

Complete chemical results for the dissolution stage leachates are tabulated in Appendix B3. The control column leachate pH, after an initial high of 4.46, rapidly stabilised at a value of 4.1-4.2 for the duration of the dissolution stage (Fig. 3.12a). This was very similar to the control column leachate pH in experiment 1. This indicates that retention of the soluble secondary phases in the waste material caused little reduction in the acid generating capacity of the waste. The pH trends of the dissolution stage coated column leachates were remarkably similar, being within 0.32 of a pH unit of each other throughout the dissolution stage (Fig. 3.12a). All coated column leachates gradually declined from pH ~7.2 to ~6.2 at the conclusion of the dissolution stage.

Conductivities of all columns were initially relatively high (550–1300 µS/cm) and dropped rapidly at first, then gradually to values of 70–100 µS/cm (Fig. 3.12b). The control column leachate conductivities were lower than the coated column leachate conductivities until near the conclusion of the dissolution stage.

The general trends of column leachate chemistry identified in experiment 1 were also present in experiment 2. Base metal concentrations in the coated column leachates were much lower than in the control column leachates, generally by an order of magnitude (Fig. 3.9d,e,g). In contrast, metalloid concentrations in the coated column leachates were higher than in the control column leachates (Fig. 3.9b,f). However, there was far more variation between the trends of individual elements than in experiment 1, particularly between coated column and control column leachate values. The concentration of SO_4^{2-} was initially high and dropped rapidly before stabilising at much lower values in all column leachates (Fig. 3.9c). The control column leachate [Fe] was below detection (0.1 mg/l) throughout the dissolution stage, whereas the coated column leachate [Fe] rose initially and then dropped below detection (Fig. 3.9h). Copper and Zn behaved similarly, control column leachate concentrations dropping rapidly from an initial high before stabilising. The concentrations of Cu

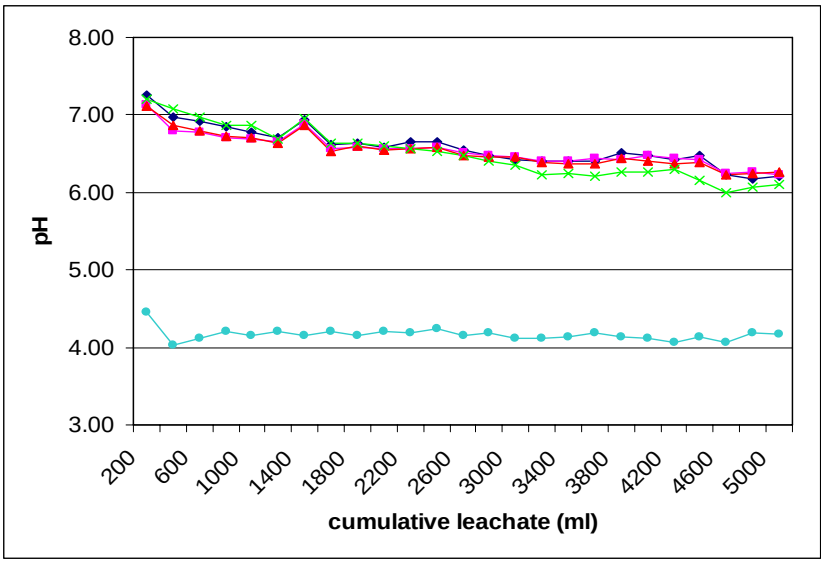

Figure 3.12a.

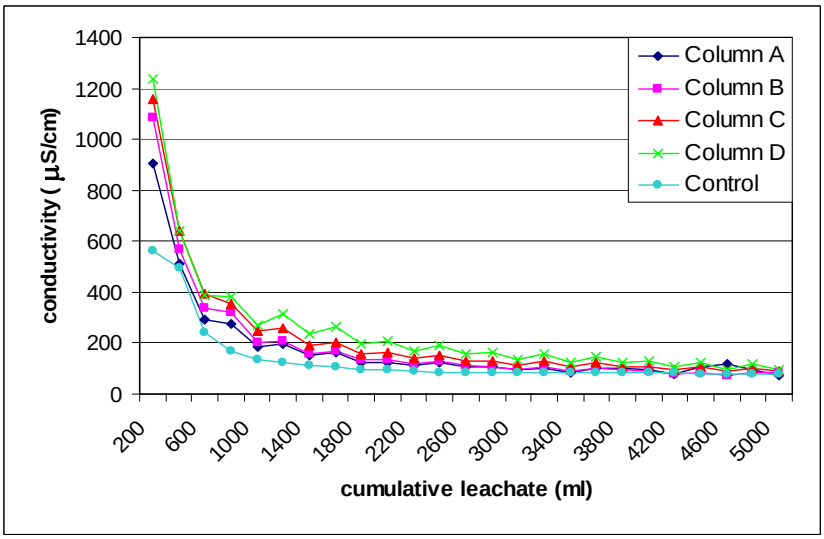

Figure 3.12b.

Figure 3.12. Experiment 2 pH (a) and conductivity (b) of dissolution stage leachates. Legend for (b) also applies to (a).

and Zn in the coated column leachates were initially low and increased steadily during the dissolution stage (Fig. 3.9d,e). In contrast, in all columns [Pb] initially rose before steadily declining (Fig. 3.9g). Control column leachate [Al] dropped rapidly after an initial high, whereas the coated column leachate [Al] rose steadily before dropping steadily (Fig. 3.9a). The control column leachate [As] remained relatively similar throughout the dissolution stage, whereas concentrations of As and Sb in the coated column leachates decreased rapidly from an initial high, then decreased steadily (Fig. 3.9b,f).

Dissolved element concentration trends of the four coated column leachates again showed very little variation between them. The exceptions were column A [Fe] and column D [Cu] and [Zn], which were significantly higher than the other respective coated column leachate concentrations (Fig. 3.9d,e,h). The relative elemental abundance in the coated column leachates of the dissolution stage (average of the cumulative element release during the dissolution stage for the four coated columns) was SO_4^{2-} > Al > Zn > Sb > As > Cu > Fe > Pb. This differs significantly from the order of cumulative elemental abundance in the control column leachates, which was SO_4^{2-} > Cu > Zn > Pb > Al > Sb > As > Fe.

SEM observations

A summary of the SEM observations (on the waste material removed from the columns at the conclusion of the dissolution stage of the experiment) is presented in Table 3.8. Detailed results and additional SEM micrographs are presented in Appendix B6. As in experiment 1, the amorphous Fe–K phosphate coatings and the various Pb phosphate phases were generally unchanged in appearance and abundance after the dissolution stage (Fig. 3.13a,b,d). However, no Fe-K phosphate coatings were observed on sphalerite after the dissolution stage. The Cu and Zn phosphate phases appeared to be reduced in abundance in all columns. The appreciable amounts of Cu, Zn, S, Si and Al often detected by EDS in the amorphous Fe-K phosphate coatings after the coating stage were only detected in column C after the dissolution stage. Evidence of corrosion of Zn phosphate crystals was found in columns B and C (Fig. 3.13c), indicating their instability in the oxidising solution. The scattered Cu phosphate rosettes appeared to have been preferentially removed in comparison to the extensive coalescences, though this may be a function of original abundance. Sulphates precipitated on phosphate phases were observed in greater variety and abundance after the dissolution stage of experiment 2 (Fig. 3.13d), implying that SO_4^{2-} was freely available within the columns.

Table 3.7. Summary of SEM observations of precipitates and coatings found on partly oxidised, polyminerallic mine waste after the conclusion of the dissolution stage of experiment 2.

Chemistry	Morphology	Abundance
Pb±Ca, K, (Cu) phosphate (Fig. 3.13d)	extensive coalescences of pincushions of fine (<1 µm) acicular crystals; large (30 µm x 10 µm) bladed and prismatic crystals; botryoids; granular precipitates; spheroids and rosettes	pincushions cover ~99 % of galena in all columns; large crystals cover ~10 % of galena in columns B and D; botryoids common in columns A and D; other phases rare precipitates in columns A, B and D
Cu±Ca-K, Fe, (S, Zn) phosphate (Fig. 3.13b)	scattered spherical rosettes up to 30 µm diameter, often extensive coalescences of radial acicular splays; amorphous flow-like coatings and tabular crystals (Cu-Zn phosphate)	heterogeneous development, cover ~100% of grains where coalesced, absent otherwise in columns A and B, also abundant on coated chalcopyrite and scattered on other minerals in columns C and D; coatings and tabular crystals on well-coated grains in column C only
Fe-K±Cu-Zn, Ca, (As) phosphate (Fig. 3.13a,b)	amorphous to flaky coating with extensive desiccation cracks, variable thickness; some disaggregated rosettes in column A	thin coating on 25 % of arsenopyrite in column A and ~75 % of chalcopyrite in column A and B; thick coating on ~99 % of chalcopyrite and stannite and thin coating on >50 % of arsenopyrite in columns C and D
Zn±Ca, K, Cu phosphate (Fig. 3.13c)	large (200 µm x 100 µm) prismatic, bladed and tabular crystals; rosettes; acicular splays; radial flow-like agglomerations of fine-grained (10 µm x 1 µm) acicular crystals; bean-shaped platelets; some crystals show evidence of corrosion	large crystals isolated precipitates in columns A and B, more common in columns C and D; flow-like agglomerations rare in column B, cover ~40 % of sphalerite in columns C and D; other phases scattered precipitates in columns C and D
Ca and K-(Cu) phosphate	fine-grained granular agglomerations (Ca); platy irregular coating (K-Cu)	agglomerations rare precipitates in columns A and B; platy phase rare coating on tetrahedrite in column C

Table 3.7 continued.

Chemistry	Morphology	Abundance
Cu, Pb, Ca, Zn, Fe sulphates (Fig. 3.13d)	euhedral rosettes; botryoidal agglomerates; platelets; dendrites; amorphous precipitates; acicular, fibrous and prismatic crystals	Cu sulphates common (cover <5 % of well-coated grains) in all columns; Pb sulphates common in column B; other phases rare precipitates

3.4.5 Discussion

Formation of phosphate phases

Phosphate formation was more extensive in experiment 2 than in experiment 1. This was particularly evident in columns A and B. The plentiful metal cations released by the dissolution of soluble secondary sulphates probably enabled the metal phosphates to achieve saturation more frequently in experiment 2. The most abundant highly soluble sulphate phases present in the mine waste were melanterite ($FeSO_4.7H_2O$) and chalcanthite ($CuSO_4.5H_2O$). Upon contact with the coating solution these minerals would have commenced dissolution, releasing Fe^{2+}, Cu^{2+} and SO_4^{2-} through the following reactions (Frau, 2000):

$$FeSO_4.7H_2O_{(s)} \rightarrow Fe^{2+}_{(aq)} + SO_4^{2-}{}_{(aq)} + 7H_2O_{(l)} \quad (3.8)$$

$$CuSO_4.5H_2O_{(s)} \rightarrow Cu^{2+}_{(aq)} + SO_4^{2-}{}_{(aq)} + 5H_2O_{(l)} \quad (3.9)$$

The released metal cations would then have reacted with the phosphate anion from the coating solution, forming Fe and Cu phosphate phases:

$$3FeSO_4.7H_2O_{(s)} + 4KH_2PO_{4(l)} \rightarrow (Fe^{3+},K)_3(PO_4)_{4(s)} + 3SO_4^{2-}{}_{(aq)} + K^+_{(aq)} + 2H^+_{(aq)} + 21H_2O_{(l)} \quad (3.10)$$

$$CuSO_4.5H_2O_{(s)} + KH_2PO_{4(l)} \rightarrow (Cu,K)PO_{4(s)} + SO_4^{2-}{}_{(aq)} + 2H^+_{(aq)} + 5H_2O_{(l)} \quad (3.11)$$

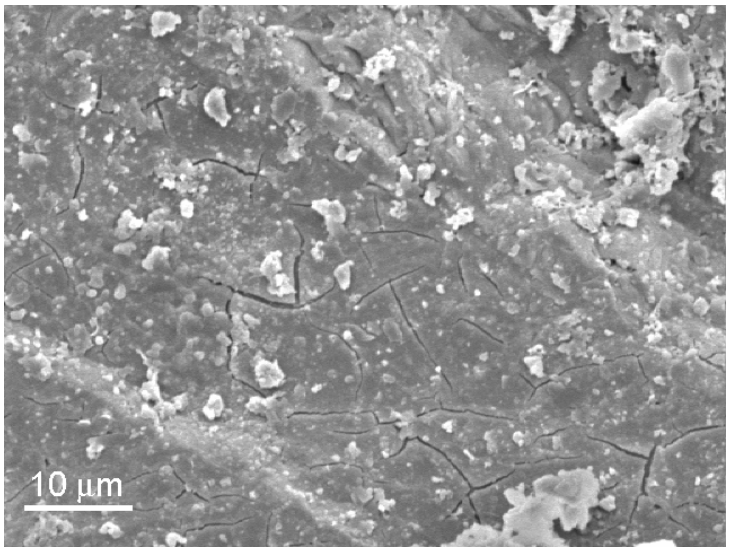

Figure 3.13a.

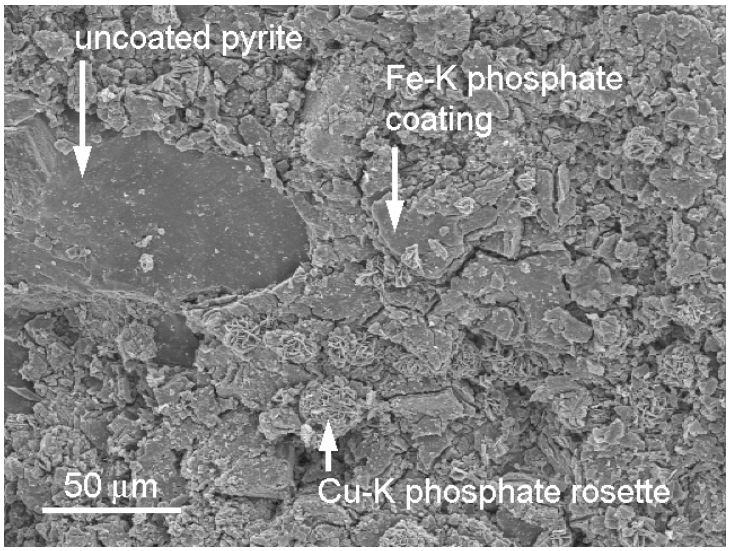

Figure 3.13b.

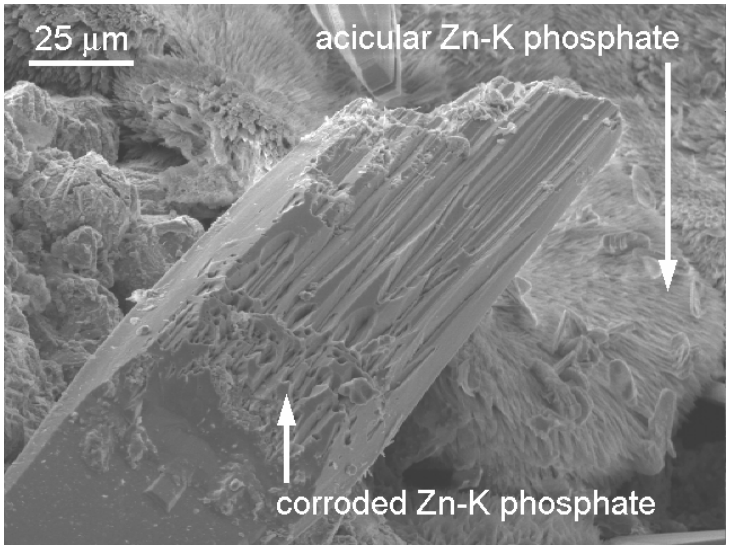

Figure 3.13c.

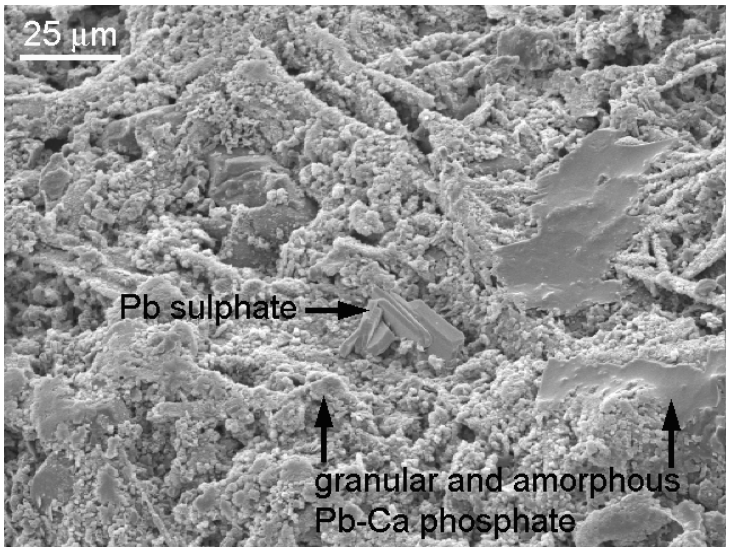

Figure 3.13d.

Figure 3.13. SEM micrographs of material removed from the coated columns after the dissolution stage of experiment 2. a) Thin, poorly developed Fe-K phosphate on chalcopyrite, column A. b) Uncoated pyrite adjacent to chalcopyrite with well-developed Fe-K phosphate coating, column C. Absence of coating on pyrite likely a result of galvanic protection by accelerated chalcopyrite oxidation. c) Tabular Zn-K phosphate crystal showing etch pits suggestive of corrosion. Acicular Zn-K phosphate in background, column C. d) Prismatic Pb sulphate crystals on amorphous/granular Pb-Ca phosphate, column D.

This process explains the observation that grains which were 100 % covered by coalesced Cu-K-Ca phosphate rosettes (Fig. 3.10b) had abundant Cu sulphates as a substrate (Section 3.4.3). Despite their extensive nature, the phosphate phases appeared to be precipitates on the sulphate substrate, with no direct interaction with the sulphate surface. This implies the sulphates dissolve and release cations into solution, which then react with the phosphate and precipitate on the grain surface, rather then the phosphate reacting with the metal within the sulphate crystal lattice. Reactions 3.10 and 3.11, coupled with the sacrificial oxidation of sulphides, explain the very high [SO_4^{2-}] in the coating stage leachates (Fig. 3.9c).

The amorphous Fe-K phosphate coatings were more abundant and well-developed on chalcopyrite and arsenopyrite in experiment 2 than experiment 1. In addition amorphous Fe-K phosphates were observed on sphalerite in columns A, B and D. The increased abundance of Fe-K phosphate coatings

was likely promoted by the increased [Fe^{3+}] through melanterite dissolution (Reaction 3.10) and subsequent oxidation of the ferrous iron. This theory is supported by the presence of amorphous Fe-K phosphates on Fe-poor sphalerite. The Fe in the phosphates on sphalerite could not be derived from the oxidation of the mineral. The phosphate probably formed as a precipitate rather than a coating interacting with the mineral surface as little Fe was present in the sphalerite lattice. The presence of substantial quantities of Zn in many of the Fe-K phosphate coatings on chalcopyrite also implies that incorporation of metals into the Fe-K phosphate coatings occurred, possibly as later precipitates.

The addition of $Ca(OH)_2$ was not necessary to induce the formation of phosphate coatings or precipitates. Fytas and Evangelou (1998) state the purpose of the $Ca(OH)_2$ was "to form calcium phosphate complexes on pyrite surfaces in order to increase phosphate coating resistance on a long-term basis". Calcium was only occasionally detected in the Fe-K phosphate coatings on chalcopyrite. The fact that oxidation was successfully inhibited despite the lack of Ca suggests that $Ca(OH)_2$ addition may be superfluous for phosphate treatment of chalcopyrite-rich mine waste. However, the substantial Ca often detected with the Cu, Pb and Zn phosphates, may have a stabilising effect on these phases. Further column experiments without $Ca(OH)_2$ addition are required to determine whether this process is required to form phosphate phases which effectively inhibit sulphide oxidation and attenuate metal release from sulphidic mine waste.

Although over 300 phosphate minerals exist in nature (Nriagu, 1983), the GADDS results of large Cu, Pb and Zn phosphate crystals formed in column D (Section 3.4.3) (Appendix B8) showed that the phases had no natural analogues. This is probably the case for the other phosphate phases formed in the phosphate stabilisation experiments, with the possible exception of pyromorphite. More sensitive analytical procedures are required to ascertain the true speciation of the metal $\pm$ alkali phosphates, particularly the very fine-grained or amorphous coatings.

The dissolved element trends in the experiment 2 coating stage leachates were similar to those in experiment 1 for all elements except As and Sb (Fig. 3.9b,f). Arsenic and Sb trends also differed from each other appreciably, which was unexpected as the aqueous chemistry of As and Sb are believed to be similar (Ashley et al., 2003). This indicates the solid phases controlling Sb and As concentrations react differently in the coating solution. The higher [Sb] in column C and D coating stage leachates (Fig. 3.9b) suggests tetrahedrite oxidation controls the [Sb] within the leachates. The reason for the steady increase in [Sb] during the coating stage is unknown. The rapid decrease in coating stage leachate [As] (Fig. 3.9f) suggests depletion of readily-mobilised As. Phosphate has been shown to rapidly replace arsenate on goethite surfaces through a ligand exchange mechanism (O'Reilly et al., 2001), which may be responsible for the high leachate [As] at the start of the coating stage. Dissolution of scorodite (Krause and Ettel, 1988) or rapid desorption of As from iron (hydr)oxides (Savage et al., 2000) at pH 5–6 are other processes possibly responsible for the observed As trends. The lower [As] during the remainder of the coating stage were probably controlled by arsenopyrite and arsenian tetrahedrite oxidation.

The major factor controlling the formation of phosphates in experiment 2 was again oxidant strength. Overall phosphate formation was more extensive than in experiment 1 due to the greater availability of metal cations through the dissolution of secondary sulphates. Processes controlling the leachate dissolved element concentrations in experiment 2 were generally the same as those of experiment 1 (Section 3.3.5). This is reflected by the generally similar elemental trends in experiment 1 and 2 coating stage leachates. However, the desorption of elements from and dissolution of secondary phases would have contributed significantly more aqueous ions to the solution.

Stability of phosphate phases

The leachate pH remained above 6 and acid generation was prevented in all of the coated columns during the dissolution stage (Fig. 3.12a). This was well above the control column value of ~4.15. However, the variable abundance of

phosphates observed in the coated columns (column D > column C >> column B > column A) did not influence the leachate pH. This implies that although the Fe-K phosphate coatings observed in columns A and B were thin and poorly-formed (Fig. 3.10a; Fig. 3.13a), they were able to prevent sulphide (particularly chalcopyrite) oxidation and hence acid generation.

The Fe-K phosphate precipitates on sphalerite and the impurities (Cu, Zn, S, Si and Al) within Fe-K phosphate coatings on chalcopyrite were absent or reduced in abundance after the dissolution stage. This implies that these phases, interpreted to have formed as precipitates from solution, were less stable in the oxidising solution than the Fe-K phosphate coatings which were reacted directly with sulphide surfaces. The Fe released from dissolution of these precipitates may be responsible for the slightly elevated Fe concentrations in the coated column leachates during the dissolution stage (Fig. 3.9h).

The concentrations of base metals in the coated column leachates during the dissolution stage were likely controlled by the stability of the base metal phosphates in the oxidising solution, although the solution pH may also have an important effect. The Pb phosphates were stable in the oxidising solution, resulting in low [Pb] in all coated column leachates during the dissolution stage (Fig. 3.9g). In contrast, the corroded Zn phosphate crystals observed in columns B and C after the dissolution stage (Fig. 3.13c) demonstrate the instability of the Zn phosphates in the oxidising solution. The corrosion of the Zn phosphates was likely responsible for the steadily increasing [Zn] in the coated column leachates during the dissolution stage (Fig. 3.9d). No direct evidence of corrosion of Cu phosphate rosettes was observed, however, their decreased abundance in the waste material after the dissolution stage implies they were unstable in the oxidising solution. The dissolution of Cu phosphates was probably responsible for the coated column leachate [Cu] increasing during the dissolution stage (Fig. 3.9e). The relatively high Cu and Zn concentrations in the column D leachates are probably due to a greater quantity of Cu and Zn phosphates being available for corrosion during the dissolution stage than in columns A and B. However, why this is not the case for the column C dissolution stage leachates is not clear.

Concentrations of As and Sb in the dissolution stage leachates are a function of solution pH. The acidity of the control column promoted metalloid attenuation as in experiment 1. The [Sb] shows a marked increase at the start of the dissolution stage in the leachates of all the coated columns compared with the coating stage leachate concentrations (Fig. 3.9b). This is possibly due to the large pH increase (pH >8) associated with the addition of $Ca(OH)_2$. The increased pH may have increased desorption of Sb from iron (hydr)oxides in the waste material. Arsenic concentration, in contrast, showed no increase in the coated column leachates at the start of the dissolution stage (Fig. 3.9f). The readily mobilised As may have already been removed from the waste material early in the coating stage.

Aluminium concentrations in the coated column leachates during the dissolution stage were probably controlled by the dissolution of sparingly soluble clays, and remobilisation of some Al from the Fe-K phosphate coatings. Though the leachate pH was above the first hydrolysis constant of Al^{3+} in all coated columns (Nordstrom and Ball, 1986), no Al-rich precipitates were observed. The initial elevated [Al] in the control column leachate (Fig. 3.9a) was probably due to the dissolution of soluble Al-bearing sulphates present in the mine waste (e.g. K-alum, tamarugite; Table 2.2). Flushing of the released Al^{3+} and rapid depletion of the sulphates led to lower [Al], possibly controlled by the dissolution of sparingly soluble clays.

The similarity of $[SO_4^{2-}]$ in the control and coated column leachates during the dissolution stage (Fig. 3.9c) poses problems for interpretation. The degree of sulphide oxidation was probably much greater in the control column than in the coated columns, as evidenced by the leachate pH values. The control column leachate $[SO_4^{2-}]$ was probably controlled by the dissolution of secondary sulphates and the oxidation of sulphides. It is possible that the amount of SO_4^{2-} released from the dissolution of secondary sulphates masked any differences in SO_4^{2-} release due to sulphide oxidation between the coated and the control columns. In addition, coprecipitation and adsorption of SO_4^{2-} onto iron (hydr)oxides may have reduced the $[SO_4^{2-}]$ in the control column leachates

(Rose and Ghazi, 1997). The initially high [SO_4^{2-}] in the coated column leachates at the start of the dissolution stage is possibly due to the dissolution of sulphates formed during the coating stage or the desorption of SO_4^{2-} from iron (hydr)oxides at the alkaline conditions (pH >8) resulting from the addition of the $Ca(OH)_2$ (Rose and Elliot, 2000).

The greater degree of amorphous Fe-K phosphate coating developed in experiment 2 inhibited the generation of acid in all coated columns. This was despite the thin, poorly-developed nature of the coatings in columns A and B. The concentration of dissolved base metals in the leachates was controlled by the stability of the base metal phosphates in the oxidising solution coupled with inhibited sulphide oxidation. Leachate metalloid concentrations were controlled by the pH of the leachate, which influenced the aqueous mobility of the metalloids.

3.4.6 Summary

The presence of secondary minerals in the partly oxidised mine waste promoted the formation of phosphate phases through the increased availability of cations for complexation with the phosphate anion. The strength of the oxidant used in the coating solutions was still the most important factor governing the extent of phosphate formation. The higher concentrations of cations in solution allowed the formation of phosphate precipitates on all sulphides to varying degrees. Chalcopyrite and galena again hosted the most abundant coatings and precipitates respectively.

The degree of phosphate formation had no effect on acid generation inhibition with acid generation being prevented in all coated columns. Base metal release was also probably inhibited by the phosphate phases, typically by an order of magnitude, although Zn and Cu release increased during the dissolution stage, likely through the dissolution of Zn and Cu phosphates.